EARLY DETECTION OF MALARIA PARASITIC RNA THROUGH AN AMPLIFICATION-FREE SURFACE-ENHANCED RAMAN SPECTROSCOPY BIOSENSOR

By

Ashley Blackwell

A thesis submitted to the faculty of
The University of North Carolina at Charlotte
in partial fulfillment of the requirements
for the degree of Master of Science in
Chemistry

Charlotte

2022

Approved by:

_____
Dr. Jerry Troutman

_____
Dr. Eugenia Lo

_____
Dr. Joanna K. Krueger

_____
Dr. Brian T. Cooper

©2022
Ashley Blackwell
ALL RIGHTS RESERVED

ABSTRACT

Ashley Blackwell. EARLY DETECTION OF MALARIA PARASITIC RNA THROUGH AN AMPLIFICATION-FREE SURFACE-ENHANCED RAMAN SPECTROSCOPY BIOSENSOR.
(Under the direction of Dr. Swarnapali De Silva Indrasekara and Dr. Jerry Troutman)

Malaria retains its position as one of the most highly transferable diseases throughout the world today, with current efforts focused on controlling its spread. A sensitive, asymptomatic-stage detection method is needed to diagnose malaria before patients begin to experience symptoms. This asymptomatic-stage method would detect the malaria parasite within its early gametocyte stage, before transmission can occur. This would eliminate transference between hosts and greatly reduce malaria cases around the world. However, the current primary diagnostic techniques for malaria detection centers around the symptomatic stage. Light microscopy is the gold standard for malaria diagnostics as it requires low cost and a quick turnaround time; however, this technique lacks sensitivity and requires skilled personnel to visualize the malaria parasite within the blood sample. Rapid diagnostic tests (RDTs), which detect malaria antigens within fifteen minutes, are also available. While these are time efficient and do not require skill to perform, they can only detect symptomatic stage malaria, similar to light microscopy, as RDTs require a high number of malaria parasites in the blood sample to be detectable. Lastly, polymerase chain reaction (PCR) can be used to detect parasitic malaria RNA sensitively but requires an extensive laboratory setup which proves to be expensive and unreasonable for in-field applications. Surface Enhanced Raman Spectroscopy (SERS) has emerged as a useful analytical method that possesses high sensitivity and selectivity. With the exploitation of SERS, this assay aims to produce a technique for asymptomatic-stage malaria detection which will be portable for point-of-care (POC) application. This system targets the

Pfs25-mRNA malaria biomarker, which is linked to gametocyte detection. We use a sandwich hybridization framework to employ reporter and capture probes with complementary nucleic acid sequences to bind to the target RNA sequence. The reporter probe is composed of a silver-coated gold nanostar (Ag@AuNS) or a silicon-coated gold nanostar (Si@AuNS) with an embedded Raman tag to serve as a signal reporter while providing SERS enhancement from the plasmonic, noble metal properties of the silver and gold. This thesis compares the enhancement achieved from utilization of rose bengal (RB), cyanine5 (Cy5), and cyanine7 (Cy7) dyes as the embedded Raman tag. A gold-coated silver nanostar (Au@AgNS) complex is also investigated as an optimized SERS substrate for this and other SERS-based assays. The capture probe currently involves the use of a magnetic bead, which is used to pull the hybridization of the three sequences out of the biological matrix. This thesis also investigates the use of a capture probe stick in comparison to the magnetic bead capture probe for a more user-friendly kit. Lastly, we aim to streamline this assay into an integrated kit consisting of a portable Raman spectrometer and the development of a machine learning model to deliver diagnostic result status through a thresholding software. Overall, this assay utilizes the sensitivity and specificity of SERS along with the portability it provides to develop a novel, practical malaria diagnostic technique which will reduce the transmission of the disease worldwide and be of use in POC application.

ACKNOWLEDGEMENTS

I will begin with thanks to my research advisors, Dr. Swarnapali De Silva Indrasekara and Dr. Jerry Troutman. Dr. Indrasekara has supported me through the trials of this project, all while assisting me in the knowledge needed about the techniques, instrumentation, and fundamental concepts. This expertise was essential in my work centering on Raman spectroscopy and nanoscale materials. Dr. Troutman has offered guidance in traversing the finality of my master's degree as well as advice on the presentation of my thesis defense. I would also like to thank Dr. Eugenia Lo for her partnership on this project and the immense biology insight added to this discourse. I would like to thank Dr. Joanna Krueger and Dr. Brian Cooper for their participation on my thesis committee and their advice concerning the trajectory of this project. Lastly, I would like to thank North Carolina Biotechnology for their generous funding of my second semester of my first year at the University of North Carolina at Charlotte. Similarly, I would also like to thank NC Space Grant Consortium and the Walsh fellowship for funding in my second year in the master's program at the University of North Carolina at Charlotte.

TABLE OF CONTENTS

LIST OF TABLES

LIST OF EQUATIONS

LIST OF FIGURES

LIST OF ABBREVIATIONS

RDT	rapid diagnostic test
PCR	polymerase chain reaction
RNA	ribonucleic acid
SERS	surface enhanced Raman spectroscopy
POC	point-of-care
Ag@AuNS	silver-coated gold nanostar
RB	rose bengal
Cy5	cyanine5
Cy7	cyanine7
Au@AgNS	gold-coated silver nanostar
P. falciparum	*Plasmodium falciparum*
P. vivax	*Plasmodium vivax*
DNA	deoxyribonucleic acid
SPR	surface plasmon resonance
LSPR	localized surface plasmon resonance
LOD	limit of detection
LOQ	limit of quantification
LDR	linear dynamic range
RP	reporter probe
CP	capture probe
TP	target probe
DFS	dark-field scattering
TEM	transmission electron microscopy
Si@AuNS	silicon-coated gold nanostar
H-buffer	hybridization buffer

CHAPTER 1: INTRODUCTION

1.1 Influence of Malaria on the World's Population

The majority of current diagnostic methodologies for infectious diseases detect the disease in the symptomatic stage.[1] While many of these diagnostic techniques have the advantage of sensitivity in this stage, detection in the symptomatic window of these infectious diseases does not prevent transmission to other hosts. Medicine is available for treatment during the detectable symptomatic stage; however, the World Health Organization notes that a gap in this field is a sensitive asymptomatic-stage detection method. Development of an asymptomatic diagnostic technique for infectious disease would not only aid in the early treatment of the disease but would also reduce the transmission to a new host. These efforts would work toward eradication of each infectious disease.[1]

Parasitic malaria remains one of the most prevalent, highly-transferable infectious diseases throughout the world.[1] The World Health Organization recorded 229 million cases of malaria throughout the world in 2019. Since the 2018 malaria case count was 228 million, this disease is increasingly spreading each year. Now more than ever, there is a need for an early detection method that will reduce the transferability of malaria.[1]

1.2 Malaria Disease and its Current Diagnostic Techniques

Malaria has proven to be most rampant in tropical regions as it is spread through the *Anopheles* female mosquito, as mentioned by Vale et al.[2,3] The *Plasmodium* parasite takes root in these female mosquitos as sporozoites, making them malaria vectors, and is transferred to a human host (Figure 1). From there, the parasite infects the human liver and targets the hepatocytes, or liver cells. The Jenner Institute not

es that replication of the parasite occurs within the liver, and the hepatocytes rupture, releasing the merozoites of the *Plasmodium* parasite. This will allow for the parasite to infect human red blood cells. [2,3]

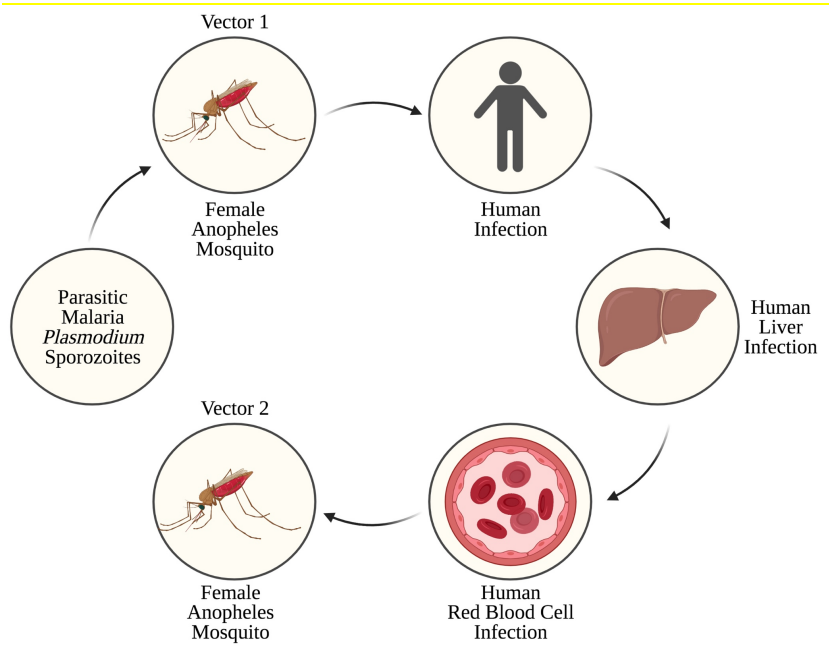

Figure 1. Parasitic malaria transmission and life cycle.[2] Created with BioRender.com.

After red blood cells become infected with parasitic merozoites, the ring stage of reproduction begins which will produce gametocytes and schizonts, as investigated by Tuteja.[4] The schizonts will rupture the blood cells and continue to wreak havoc inside the human body while the gametocytes continue to mature into males and females, which will sexually produce zygotes. These zygotes will be ingested by another mosquito through a bite that will transfer the infected human red blood cells. This mosquito then becomes a new malaria vector to continue transmission.[4]

The parasite life cycle repeats until treatment intervenes or until all or most red blood cells are infected with the malaria parasite, resulting in death.[4] Tuteja also notes that when there are more than 40 parasites in a single microliter of blood, the patient will begin to experience

symptoms as more red blood cells are becoming infected. This is the beginning of the symptomatic stage. Currently, diagnostic techniques concentrate on the symptomatic stage of the malaria life cycle.[4]

Blood smear microscopy is considered the gold standard of malaria detection. A patient blood sample is stained using a Romanovsky dye, typically Giemsa.[5] This dye will bind to the parasitic malaria ribonucleic acid (RNA). The stained blood is analyzed through light or fluorescence microscopy. Fluorescence microscopy will observe a fluorescent response from the stained parasite if present. Hathiwala et al. developed a light-emitting diode (LED) fluorescence microscopic technique which reported 86 out of 300 samples positive compared to 111 out of 300 positive samples using light microscopy. This demonstrates the variability in microscopic techniques. Out of these, light microscopy is more widely used. Light microscopy relies on the simple visual cues of the dye in the blood cells to determine the presence of the parasite.[5]

Most malaria microscopy techniques begin with a thick blood smear from the stained sample, as there will be more parasites present in the thick smear. This is used to determine if parasites are present within the patient sample, and a positive or negative result is assigned. From there, a thin blood smear is performed using the same stained patient blood sample. This thin smear is analyzed using a 100X oil objective to determine the percent of infected red blood cells as well as the species of parasite present, as there are five.[6] The five malaria species include *Plasmodium falciparum (P. falciparum), Plasmodium malariae, Plasmodium vivax (P. vivax), Plasmodium ovale, and Plasmodium knowlesi,* with *P. falciparum* and *P. vivax* causing the majority of malaria cases across the world.[7]

Blood smear light microscopy is the most widely used technique for malaria detection as it is an established method with a low cost, as any laboratory with a hematology-grade

microscope can perform this. This method also provides results within an hour, though this becomes a disadvantage as well. Light microscopy malaria testing is recommended by the Center for Disease Control (CDC) to be performed within hours from collection. The test must also be performed by a qualified technician in order to be considered reliable. This creates a hindrance as not every lab in resource-limited areas possesses a qualified technician to observe the sample. There is also a lower limit on the sensitivity achievable by light microscopy, as there needs to be roughly 100 parasites per microliter of blood. This falls outside of the early detection window.[6]

Recently, Rapid Diagnostic Tests (RDTs) have become a widely used technique for the detection of malaria. The RDT is antibody based, with current tests capturing three malaria antigens: *Plasmodium* histidine-rich protein, *Plasmodium* lactate dehydrogenase, and *Plasmodium* aldolase.[8] Blood samples are collected from patients and dropped onto the nitrocellulose testing card, along with the required reagents – including labeled indicator antibodies. The patient specimen then moves down the strip to the capture antibodies. Once captured through a different epitope than the indicator antibody, the indicator antibody complexed to the antigen will form a line on the testing card, indicating a positive malaria result.[8] RDTs only require fifteen minutes for the results to become available. However, the CDC recommends that RDTs only be used as an initial diagnostic test, which must be followed by microscopy for a final malaria diagnosis.[6]

RDTs also require over 100 parasites per microliter of blood, which disqualifies the detection of the early, asymptomatic-stage using this technique. RDTs test for two antigen types, one specific to *P. falciparum* and the other found in four of the human malaria species. Therefore, light microscopy must be used to determine the species of parasite present in the

sample. This also further eliminates this method for early detection as the malaria infection will be well into the symptomatic stage before proteins are detected.[6]

Lastly, the Polymerase Chain Reaction (PCR) has become a widely used method for malaria diagnosis that is proven to be sensitive and specific. Johnston et al. produced a study which compared nested PCR to light microscopy of patient blood samples. The study concluded that PCR detected as low as 10 parasites per microliter of blood, which fell within the window of early detection.[9] The PCR technique amplifies the deoxyribonucleic acid (DNA) or RNA present in a sample after the denaturization step, which is the separation of DNA into single strands. Enzymes then copy the original DNA present 30 or 40 times, producing a high DNA count. Most commonly, electrophoresis is then used in combination with a fluorescent dye to quantify the PCR product.[10]

The PCR amplification technique is advantageous as RNA is the biomarker most suitable for early detection, as it is the first biomarker produced from the parasite. As stated, this qualifies PCR as an early detection method that is highly specific. However, PCR requires a full laboratory setting with skilled technicians. Since this technique requires extensive equipment, the cost to set up this equipment is high and unrealistic to do in resource-limited areas. This makes PCR impracticable as a technique for point-of-care (POC) application.[10]

1.3 The Use of Biosensors for Nucleic Acid Detection

The current diagnostic methodologies for malaria detection indicate the importance of biosensors within the medical field. A biosensor is defined as a system which uses biomarkers or living organisms for the detection of a target disease or compound.[11] Key characteristics that are vital for biosensor success for infectious diseases are sensitivity, specificity, and quick timed

testing capabilities. For optimal use, a biosensor must meet these criteria while also offering portability and cost-effectiveness to be used in resource-limited areas in POC application.

Proteins and nucleic acids have become the most frequent biomarkers to be targeted by biosensor development due to the achievable selectivity, though lipid and carbohydrate detection is also possible. The beginning stage of biosensor development is biomarker determination. From there, a schematic for detecting the specific targeted biomarker in question must be designed. This design must include a method to capture the biomarker as well as produce a signal when it is present in the matrix.[12]

As mentioned, nucleic acids are a repeatedly targeted biomarker, not only due to the unique recognition for each target but also due to the early detection capabilities. Poon et al. used a loop-mediated isothermal amplification technique to detect malaria *P. falciparum* DNA with a sensitivity comparable to PCR.[13] As DNA/RNA is the genetic coding agent to produce all other biomarkers, detection of these nucleic acids will produce the earliest detection of the presence of the target disease. DNA detection will accomplish detection of the earliest stage of these diseases and much research is devoted to the development of hybridization assays.

In 2010, Halas et al. used surface enhanced Raman spectroscopy (SERS) to detect label-free DNA.[14] The group used SERS to detect the adenine nitrogenous base at a Raman shift of 736 cm^{-1}. Using an adenine-free DNA probe complementary to the target DNA, the group was able to detect the DNA hybridization with high specificity. Another method that shows promising nucleic acid detection capabilities is the sandwich hybridization assay. This assay type involves a two-part probe system, with both probes containing different DNA sequences that are partially complementary to the target DNA, as seen in Figure 14. Most commonly, one probe will be used for separation of the hybridization scheme from the biological matrix while the

other probe is used to produce a signal for detection of said hybridization. This method is highly valued as it has the specificity to only observe a signal if the target DNA is present, with no contamination in signal from other DNA present.[15]

This sandwich hybridization-based assay type was used in work performed by Vo-Dinh et al.[16] This group used the nanorattle-based method, which employs magnetic beads with complementary sequences as the capture probe and SERS-based nanorattles with complementary sequences as the reporter probes. The nanorattles involve a core-gap-shell layout that traps the Raman dye between the core and shell as the signal reporter. This group targeted the *P. falciparum* malaria species *PF3DJ_1343J00* gene with a limit of detection (LOD) of 100-attomole.[16] The sandwich hybridization assay, as demonstrated in this literature, is innovative as it offers sensitivity with no DNA amplification. This allows this DNA recognition system to rival PCR, as it offers the sensitivity needed for early detection along with the portability to service resource-limited areas. This method does not require sample purification to control DNA contamination, like PCR does.

With nucleic acids being the ideal biomarker for early detection, it is also important to target DNA/RNA sequences that are associated with the beginning life cycle of the disease. DNA that is present at the early life stage of diseases will offer the earliest determination that the disease is present. For malaria, the Pfs25 and Pvs25 genes have been linked to the early life stages of the parasite. Specifically, the Pfs25-mRNA is associated with gametocyte production.[17] Recall that gametocytes are the result of reproduction of the malaria parasite in the ring stage and are needed for maturation into the sexual reproduction stage. Since gametocyte production is needed to produce zygotes, which is the stage in which malaria is passed onto the next vector for transmission, gametocyte detection is synonymous to asymptomatic-stage malaria detection.[4]

Therefore, if an assay can detect the Pfs25 mRNA, it will theoretically be able to detect the asymptomatic-stage of the malaria infection.

The asymptomatic-stage of malaria is classified as 40 or fewer parasites per microliter of patient blood. Since the volume of parasites in the blood is low at this stage, it is not yet capable of transference to a new host. The infection must enter into the symptomatic stage to be contagious.[18] Detection methodologies targeting the asymptomatic-stage of infection will reduce transmission. A developed malaria biosensor that can target the parasitic Pfs25-mRNA, which encodes for the Pfs25 protein linked to gametocyte production, will be optimal for early detection application.[19]

1.4 Surface-Enhanced Raman Spectroscopy (SERS) and its Detection Capabilities

The Raman effect was discovered in 1928 by Professor C. V. Raman as he sailed from London to Bombay. Professor Raman observed the blue color of the Mediterranean sea and rejected Lord Rayleigh's conclusion that the sea color was a reflection of the sky.[20] This placed Professor Raman on the path to discover Raman scattering, which is inelastic photon scattering. The inelastic scattering of a photon when light is incident upon a compound will cause an energy exchange as well as a directional change. The energy exchange will result in either a loss or a gain in energy by the molecule. Stokes Raman scattering involves the molecule gaining energy while the photons shift to a lower energy level (Figure 2). Anti-Stokes Raman is the opposite of this, with the molecule losing energy. Since anti-Stokes Raman scattering would require the molecule to already be in an excited state, the type that is typically observed in common Raman spectroscopy is Stokes Raman scattering.[21]

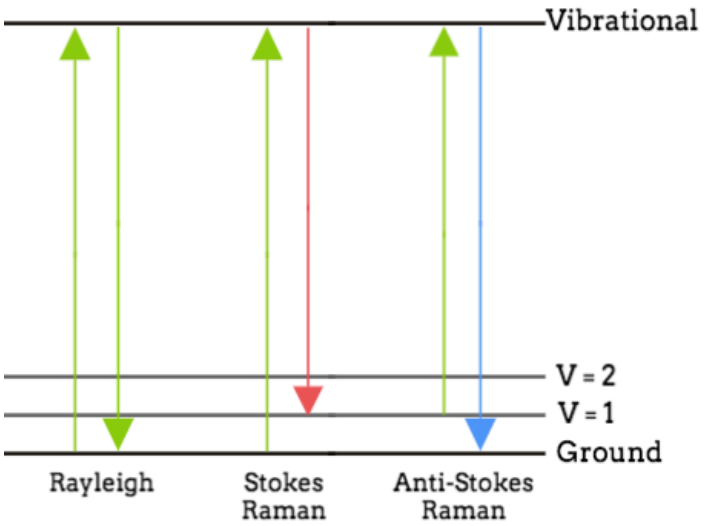

Figure 2. Jablonski diagram of Rayleigh and Raman light scattering.[21, 22]

The energy exchange experienced from the incident light source to the exit from the molecule is typically expressed as vibrational energy. The vibrational energy increase or decrease correlates to the electronic ground state of the compound. Due to this, the Raman shifts are a quantification of the vibrational energies of specific functional groups within the desired analyte. This makes Raman spectroscopy an optimal analytical technique for detection of targeted compounds or biomarkers, as each molecule will have a unique Raman fingerprint. Though the Raman effect is valuable for its sensitivity and specificity, its drawback is the frequency of inelastic photon scattering. Only about 1 in 10 million photons inelastically scatter, which makes the Raman effect inherently weak. To counter this, enhancement of this signal has been explored.[22]

Surface enhanced Raman scattering (SERS) is a technique used to enhance the Raman effect. SERS benefits from the sensitivity and specificity that unique Raman spectral fingerprints provide while enhancing the original signal through a SERS substrate that experiences two enhancement types. Electromagnetic enhancement stems from light localization, which will lead to the surface plasmon resonance (SPR) or localized surface plasmon resonance (LSPR) effect.

This resonance effect will hinge on the SERS substrate material and the electron oscillations that occur when interacting with the light source. Since the electron-light interaction is the source of this enhancement, plasmonic materials are most commonly used for SERS substrates.[23]

The second enhancement type is chemical enhancement. This occurs when the target analyte is within a 5 nanometer or less distance from the SERS substrate surface. When this occurs, a transfer of charge will transpire between the analyte and the metal of the SERS substrate or the light will be polarized dependent on the analyte. This enhancement will affect the Raman fingerprint produced for the analyte detection. Influential aspects to consider for this chemical enhancement include the excitation wavelength of the analyte, the composition of the analyte, analyte size, and the distance of the analyte and SERS substrate interface.[24]

In combination, the consideration of the electromagnetic and chemical enhancement factors constitutes the SERS enhancement. Therefore, SERS enhancement takes the SERS substrate and analyte into consideration. Typical SERS enhancement will increase the original Raman signal by 10^5-10^8, with some accounts[25] as high as 10^{12}. This SERS enhancement factor can be calculated to determine the viability and success of a given SERS substrate, where I_{SERS} and I_{Raman} are the intensities at a selected Raman shift correlating to SERS and Raman mode, respectively. N_{Raman} and N_{SERS} are the number of molecules of analyte in each system. (Equation 1).[26]

$$\text{Enhancement Factor} = (I_{SERS}/I_{Raman}) \times (N_{Raman}/N_{SERS}) \quad \text{Eq. 1}$$

SERS detection can be classified into two formats: direct and indirect. Direct detection involves the target analyte absorbing onto or being in necessary proximity to the SERS substrate, and the target analyte will serve to report the signal in the assay.[27] Zhang et al. use gold

nanoparticles as a SERS substrate for the direct detection of pesticides.[28] The gold nanoparticles were converted to microarray films and applied as a cover over foods where the nanoparticles detected carbendazol and parathion pesticide compounds.[28] Indirect Raman detection involves the use of a reporter tag or dye which will produce a Raman signal when the target analyte is present. An example of this is in the sandwich hybridization assay where a Raman tag is used as the reporter probe which will only be present in the final measured solution if the hybridization was successful. This would confirm the presence of the target molecule.[27] This technique was utilized by the Mirkin group, who used gold nanoparticles as a SERS substrate with a Raman tag attached to its surface under a silver coating. An oligonucleotide sequence was attached to this SERS substrate to capture DNA. This group compared six DNA targets and six Raman tags, with the common limit of detection for this method at 20 femtomolar.[29]

SERS detection has extended to infectious disease diagnostic methodologies. Within this category, malaria detection has become a popular SERS research topic in recent years. Zhao et al. use direct SERS for the detection of human red blood cells infected with the malaria parasite in comparison to healthy red blood cells.[29] This method utilizes silver nanorods as the SERS substrate, and a difference in the Raman spectra was observed between the healthy and infected red blood cells as the infected produced a peak at 1599 cm^{-1}.[30] Liu et al. monitored the presence of hemozoin, a malaria metabolite byproduct, with silver-coated iron oxide nanoparticles.[31] A magnetic field is applied to enrich the hemozoin and promote binding for overall direct SERS detection.[31] Mhlanga et al. produced a direct SERS assay utilizing Raman tag labeled silver nanoparticles to detect *P. falciparum* malaria proteins.[32] Lastly, Vo-Dinh et al. exploited the nanorattle indirect SERS method in a sandwich hybridization scheme to capture the 18S rRNA malaria RNA gene with embedded Raman tags serving as the reporter.[16] Time and again, SERS

is proven to be a specific detection technique that challenges PCR in sensitivity and outperforms it in portability for POC applications.

1.5 Plasmonic Materials and Noble Metals for Biosensing

In recent years, plasmonics has emerged as an informative technique which can be used to detect analytes near the plasmonic material surface. A plasmonic material is defined as a substance which possesses an electron density able to interact with light and produce an electromagnetic field. This electromagnetic field production is due to the free electron oscillation around the plasmonic material that occurs after the light interaction. Once this electromagnetic field is created, it can scatter new light with more, less, or the same energy as the incident light. This phenomenon creates the SPR effect.[33]

Plasmonic materials are sensitive to other substances in their proximity due to their oscillating surface plasmons. This can be exploited to detect certain compounds or specific binding near the plasmonic surface. Marinakos et al. used gold nanorods as their plasmonic material, to which they conjugated biotin.[34] The biotin was used to capture the streptavidin protein, and UV/Vis characterization was used to monitor the shift in wavelength emitted from the gold nanorods. This shift was due to the difference in the refractive index before and after the biotin-streptavidin binding.[34] Guo et al. also demonstrate the use of a gold substrate for SPR biosensors with the addition of a graphene coating.[35] This group compiled previously completed work using graphene coated gold to determine that an SPR biosensor of this type could be used to detect the Covid-19 virus.[35] Gold and silver are the most commonly used materials for plasmonics; however, platinum, gallium, aluminum, and magnesium are other elements with this capability as well as metal oxides, graphene, and other semiconductor materials.[36, 37]

Though plasmonic materials are advantageous for their detection capabilities, they also suffer a disadvantage from the bulk effect (Figure 3). The surface plasmons will propagate from the material as a wave, making the strongest point of the electromagnetic field at the surface of the plasmonic material. However, the propagation of these waves will extend 250-1000 nanometers when the material is in a film. This will detect unwanted analytes that are far from the plasmonic material surface, causing the bulk effect. When the plasmonic material is in the shape of a nanoparticle, which interrupts the continuous electromagnetic wave propagation, the waves only extend 20-40 nanometers from the surface of the plasmonic material. This creates the LSPR which experiences a negligible influence from the bulk effect.[38, 39]

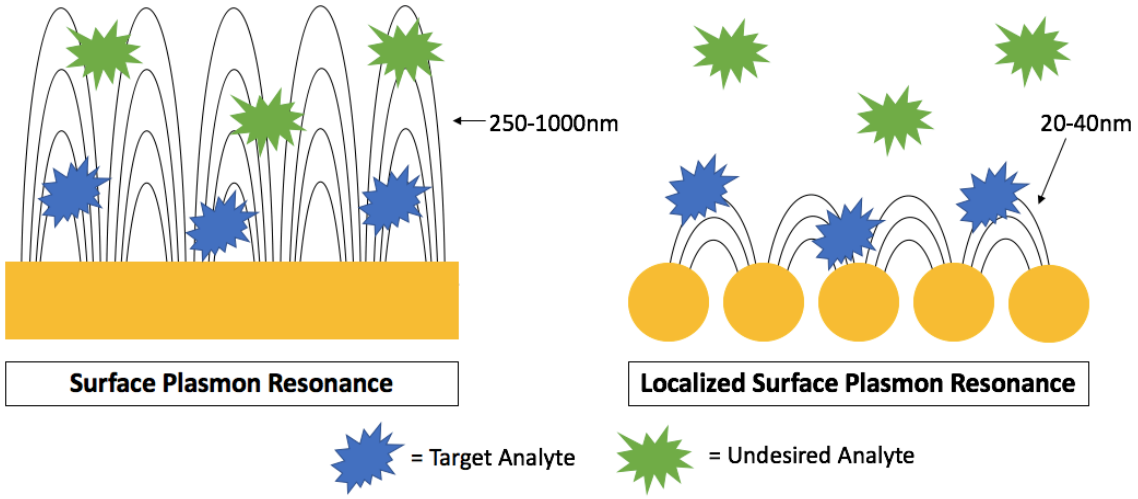

Figure 3. The bulk effect influence on Surface Plasmon Resonance and Localized Surface Plasmon Resonance.

As gold and silver are the most common plasmonic materials, their physical and optical properties have been highly studied.[41-44] Gold and silver fall within the noble metal category (Table 1). A noble metal is chemically classified as a material that is resistant to oxidation and corrosion while it is physically defined as an element that has a filled electron d-orbital.[40] Noble

metals are recognized for their unique physiochemical and optical properties compared to base metals. These properties are highlighted with the gold and silver elements. Gold shows optimal physiochemical properties of simple functionalization chemistry and resistance to corrosion and oxidation.[41] Silver possesses a high efficiency of light scattering and absorbance.[42] These properties, combined with their plasmonic capabilities, make silver and gold optimal materials to utilize for biosensing substrates. The combination of shape dependence and elemental dependence for an optimized plasmonic substrate displays a gold or silver nanoparticle as the most efficient and enhanced substrate type (highlighted in Table 1).

Table 1. Properties of Noble Metals and their Plasmonic Capabilities for Biosensing[43, 44]

Metal	Notable Properties	Plasmonic in UV/Vis Region
Ruthenium (Ru)	Unaffected by acids, water, and air	None
Rhodium (Rh)	High reflectance	None
Palladium (Pd)	Low melting point, not oxygen-reactive	Weak
Osmium (Os)	High melting point, "hard"	None
Iridium (Ir)	Most corrosion resistant, high density	None
Platinum (Pt)	Highly resistant to oxidation, "soft"	Weak
* Copper (Cu)	Good corrosion resistance	Medium
Gold (Au)	Highly resistant to oxidation & corrosion	Strong
Silver (Ag)	High absorbance and scattering efficiency	Strong

* Copper is considered a noble metal by the filled electron d-orbital definition, but not by the oxidation-corrosion definition.

1.6 Development of an Optimized SERS Substrate

As previously discussed, a silver or gold nanoparticle will experience noble metal, plasmonic characteristics while benefitting from a negligible bulk effect. Their nanoparticle shape will benefit from the LSPR effect instead of SPR. Though a spherical-shaped nanoparticle

will experience the LSPR effect, SERS enhancement is increased when the analyte is positioned near edges, tips, or crevices of the SERS substrate metal. This creates a SERS hotspot.[27] Due to this, nanostars provides a high SERS enhancement compared to spherical particles. In addition to this shape dependence, there is a size dependence that must be met in order to profit from the LSPR effect. The size of this nanoparticle must be smaller than the incident light wavelength.

While independent plasmonic metal nanoparticles provide heightened signals, nanoparticles with a core shell and bimetallic coating have shown tremendous SERS enhancement capabilities.[45] This design will allow for the utilization of properties from both materials. For example, a gold-coated silver nanoparticle will benefit from the chemically stable gold coating as well as a higher LSPR with the efficient optical properties from the silver core. Alterations and combinations of materials as coatings and cores will determine the distinctive properties of each SERS substrate.[46]

A core-shell nanoparticle also provides the capability to embed a Raman tag to use as a signal reporter. In comparison, an external Raman tag would compete with additional absorbing molecules, perhaps even the target molecule. Embedment will also decrease surface adsorption and variation as well as increase the overall reproducibility of the substrate.[47] Since SERS substrate reproducibility is a large obstacle in this field, a core-shell nanoparticle with an embedded Raman tag is an improvement. The choice of Raman tag is also crucial, as a Raman tag with an excitation peak that is in resonance with the incident laser wavelength will produce a higher SERS enhancement.

1.7 Characterization Methods for Nanoparticles

The process of synthesizing nanoparticles for a SERS substrate requires several characterization techniques. UV/Vis characterization can be used as an initial step to relatively indicate the excitation peak of a nanoparticle. This will directly correlate to its size and can be used to determine if the batch is a failure or should move onto the next characterization. Concentration of the nanoparticles in solution can also be obtained from UV/Vis spectra in combination with Beer's law.

Dark-field scattering (DFS) and transmission electron microscopy (TEM) can be interchanged as the second characterization step for nanoparticle synthesis confirmation. DFS can be used to determine the optical properties of the nanoparticle as well as generalize the uniformity and size of the sample. TEM can be used to confirm the morphology of the sample as well as size, uniformity, and degree of aggregation.

1.8 Thesis Overview

This thesis will present the findings of our investigation into a SERS biosensor for the indirect detection of parasitic malaria RNA. More specifically, we employ a sandwich hybridization-based assay. This assay utilizes a reporter and capture probe that works to trap and detect the Pfs25-mRNA malaria biomarker, as it is linked to gametocyte detection.

Our reporter probe (RP) consists of a silver-coated gold core-shell nanostar (Ag@AuNS) with a Raman tag embedded for signal reporting. This substrate will benefit from a bimetallic, nanostar structure that will provide a high SERS enhancement. This thesis also compares the use of rose bengal (RB), cyanine5 (Cy5), and cyanine7 (Cy7) as the Raman tag in the reporter probe.

We also propose and investigate an alternative SERS substrate, gold-coated silver nanostars (Au@AgNS), as it shows promise for a longer substrate shelf-life.

The capture probe consists of a magnetic bead linked to the complementary DNA sequence to pull the hybridization scheme from the biological matrix. The synthesis of the capture probe is optimal as it utilizes click chemistry and is spontaneous at room temperature. These conditions will be ideal for mass production of capture probes once the integrated kit is complete for in-field application.

Our aims include: (1) the optimization of a nucleic acid detection system targeting Pfs25 in infected blood, (2) development of Au@AgNS as a SERS substrate to optimize stability, and (3) development of an integrated platform for in-field application.

CHAPTER 2: MATERIALS AND METHODS

2.1 Materials

Reagents used in this work are as followed: gold (III) chloride trihydrate, gold (III) chloride solution, hydrochloric acid, sodium hydroxide, hydroxylamine, ammonium hydroxide, L-ascorbic acid, silver nitrate, trisodium citrate dihydrate, Rose Bengal Dye (95%), Cyanine5 PEG Dye, Cyanine7 PEG Dye, polyethylene glycol (PEG, MW: 5000). These were purchased from Sigma-Aldrich.

Additional reagents needed for the reporter and capture probe syntheses were: tris(2-carboxyethyl)phosphine hydrochloride (Thermo Fisher Scientific), tris(hydroxymethyl)aminomethane-diaminoethanetetraacetic acid (TE, Sigma Aldrich), synthetic capture/reporter sequences (Integrated DNA Technologies), phosphate buffered saline (PBS, Thermo Fisher Scientific), tween20 (TW20, Thermo Fisher Scientific), Dynabeads M-270 (magnetic beads, Thermo Fisher Scientific), dimethyl sulfoxide (DMSO, Sigma Aldrich), Dibenzocyclooctyne-N-hydroxysuccinimidyl ester (DBCO-NHS, Santa Cruz Biotechnology), and Ultrapure DNAse/RNAse free water (Thermo Fisher Scientific).

Additional reagents needed for the hybridization reactions: saline-sodium citrate (SSC, Promega), sodium dodecyl sulfate (SDS, Sigma Aldrich), and bovine serum albumin (BSA, Sigma Aldrich).

Containers for the mentioned reagents during reactions included Erlenmeyer flasks and scintillation vials. The stir bar and stir/hot plate used for all reactions was obtained from VWR. For magnetic separation of the hybridization, DynaMag™-2 Magnet was obtained from Thermo

Fisher Scientific. Additional materials needed for reactions included: 2 mL microcentrifuge tubes and VWR pipettes.

Instrumentation used for syntheses and characterization include: Horiba XploRA ONE™ Raman microscope, Cytoviva. Hyperspectral Imaging system, Thermo Scientific™ Sorvall™ Legend™ X1 centrifuge and micro 21R microcentrifuge, Thermo Scientific™ thermal mixer, Branson 2800 ultrasonic cleaner, vortex-genie 2 from Scientific Industries, and a VWR-164AC balance.

2.2 Citrate-capped Spherical Gold Nanoparticle (AuNP) Synthesis

The synthesis of 12 nm AuNP began with the addition of 194 mL of Milli-Q water to an Erlenmeyer flask. To that, 1 mL of 10 mg/mL $HAuCl_4$ was added and the solution was stirred while being heated to a boil. The stirring speed was set so that the vortex did not collapse onto the stir bar. Added to the solution after 5 minutes of boiling was 5 mL of 1% citric acid trisodium salt. The flask was covered with foil, and the solution boiled for 30 minutes. A color change to red was observed after 30 minutes. The red color determined the finality of the synthesis and the production of AuNPs. Boiling continued for 30 more minutes. In the same stirring conditions, the solution was cooled to room temperature. This mixture was centrifuged at 10,000 g for 60 minutes and resuspended in 20 mL of Milli-Q water. The final solution was refrigerated.

2.3 Silver-coated Gold Nanostar (Ag@AuNS) Synthesis

AuNS synthesis was performed by adding 984 µL of 5.08 mM $HAuCl_4$ to 10 mL of MilliQ water in a glass scintillation vial, stirring at 460 rpm at room temperature for 10 seconds. 40 µL of 1N HCl was added and allowed to mix for 10 seconds. 346 µL of 12 nm AuNP seeds

($A_{521.5}$ = 2.293 from Nanodrop) was added and mixed for another 10 seconds. 68 µL of 3 mM silver nitrate was added to the resultant solution and allowed to mix for 5 seconds. This was followed by the addition of 200 µL of 100 mM L-ascorbic acid. The solution turned blue within seconds. This solution was stirred for 1 minute under the same stirring conditions at room temperature. The resultant solution was centrifuged at 3000g for 8 minutes and resuspended in 3 mL of MilliQ water. For long term use, the solution was stored in the refrigerator.

2.4 Silicon-coated Gold Nanostar (Si@AuNS) Synthesis

AuNS synthesis was performed by adding 984 µL of 5.08 mM $HAuCl_4$ to 10 mL of MilliQ water in a glass scintillation vial, stirring at 460 rpm at room temperature for 10 seconds. 40 µL of 1N HCl was added and allowed to mix for 10 seconds. 160 µL of 12 nm AuNP seeds ($A_{521.5}$ = 2.293 from Nanodrop) was added and mixed for another 10 seconds. 68 µL of 3 mM silver nitrate was added to the resultant solution and allowed to mix for 5 seconds. This was followed by the addition of 200 µL of 100 mM L-ascorbic acid. The solution turned blue within seconds. This solution was stirred for 1 minute under the same stirring conditions at room temperature. To this, 10 mL of the 0.2 M CTAB capping agent was added to AuNS solution to stir for 30 minutes. The resultant solution was centrifuged at 3000g for 10 minutes and resuspended in 40 mL of MilliQ water. To this, 5.3 mM TEOS was added and stirred for 1 hour then 10 µL of NH_4OH was added to stir for an additional hour. Centrifugation was performed at 3500g for 30 minutes and the solution was resuspended in 5 mL of water.

2.5 Functionalization of Rose Bengal and Cyanine5 Dye onto Ag@AuNS

Onto previously synthesized AuNSs, RB or Cy5 dye was surface functionalized as a Raman tag. Based on the surface area ratio of AuNS to dye, the functionalization was performed at 60% surface saturation. The 3 mL of AuNSs was diluted to 30 mL with MilliQ water. The dye was added to this solution and mixed for 3 hours at 580 rpm under room temperature with foil covering the entire flask. Silver coating protocol was then performed by adding 120 µL of 0.05 M silver nitrate and 120 µL of 0.1 M ascorbic acid simultaneously. Immediately following, 60 µL of 28.5% ammonium hydroxide solution was added to the flask. This solution mixed for 5 minutes at 700 rpm under room temperature. There was a color change over time. RB changed from pink to brown. Cy5 changed from light blue to orange-green. While mixing, 1.2 mL of 1 mg/mL PEG-SH (5000) was added and the solution mixed for another 30 minutes. The resultant solution was centrifuged for 10 minutes at 2000g. The final solution was resuspended in 3 mL MilliQ water and characterized using UV/Vis, DFS, and TEM.

2.6 Functionalization of Cyanine7 Dye onto Si@AuNS

Onto previously synthesized AuNSs, Cy7 dye was surface functionalized as a Raman tag. Based on the surface area ratio of AuNS to dye, the functionalization was performed at 60% surface saturation. After the addition of CTAB as the capping agent, 750 µL of Cy7 PEG dye was added to the solution to mix for 15 minutes. After this, the TEOS and NH_4OH was added as previously described in section 2.4.

2.7 Silver Nanostar (AgNS) Synthesis

To a plastic scintillation vial, 500 µL of 0.13 M hydroxylamine and 500 µL of 0.05 M sodium hydroxide was added simultaneously. This solution stirred at 600 rpm. While stirring, a solution of 9 mL of 1.1 x 10^{-4} M silver nitrate was added dropwise. This addition continued at a rate of 50 µL/second. Once all of the silver nitrate was added, the solution was stirred for 5 minutes, and 100 µL of 0.03 M trisodium citrate was added. This solution was covered with a lid and mixed uninterrupted for 24, 48, or 72 hours. After mixing, 40 µL of 1 mg/mL PEG was added and mixed for 10 minutes while stirring. This solution was centrifuged at 3,500 for 10 minutes and resuspended in 1 mL of Milli-Q water. This solution was refrigerated.

2.8 Reporter Probe Functionalization

The reporter probe (RP) sequence volume used was based on 60% surface saturation of the sequence onto the Raman tagged AuNS. 42.8 µL of 100 µM thiolated synthetic mRNA reporter probe sequence was added to a microcentrifuge tube along with 5 µL of 100 mM TCEP in TE 1X. This solution was mixed on the thermal shaker for 1 hour at 700 rpm (23 ºC). To this, 1 mL of Cy5 PEG SERS substrate was added to mix for 1 hour at 700 rpm (23 ºC). Then, 10 µL of citrate-HCl buffer (300 mM trisodium citrate, pH adjusted to 3.1 using 1 M HCl) was added to mix for 1 hour at 700 rpm (23 ºC) to promote loading of synthetic mRNA onto the SERS substrate. This solution was centrifuged for 5 minutes at 6,500 rpm and resuspended in 50 µL of PEG-SH (5000) and 1 mL of PBS 1X with 0.01% TW20. This was sonicated for 2 minutes and centrifuged for 5 minutes at 6,500 rpm. The resultant solution was resuspended in 1 mL TE 1X and centrifuged again at 6,500 rpm for 5 minutes. The final solution was resuspended in 500 µL

TE 1X and characterized using UV/Vis and SERS. For long term use, this solution was stored in refrigerator.

2.9 Capture Probe Functionalization

Dynabeads M-270 magnetic beads were allowed to warm to room temperature 15 minutes before use. 22 µL of the magnetic beads were washed with 1.5 mL of DMSO 3 total times with 13.4 µL of a 1.5 mg of DBCO-NHS linker in 10 mL DMSO solution added. This solution was mixed on a thermal shaker for 1 hour. This solution was washed 3 times with 1.5 mL of Ultrapure water and resuspended in 500 µL of Ultrapure water. 75 µL of 100 µM capture probe sequence was placed in a microcentrifuge tube with 500 µL of PBS 1X buffer. This DNA sequence solution was mixed with the magnetic bead solution and mixed for 1 hour. This was then refrigerated for 18 hours. The magnetic pellet was concentrated and the supernatant removed. The pellet was resuspended in 1 mL PBS 1X buffer. This was placed in a new microcentrifuge tube. This solution was washed 3 times with 1 mL PBS 1X buffer. The final pellet was resuspended in 1 mL PBS 1X buffer.

2.10 Synthetic Pfs25-mRNA Target Hybridization in Buffer

Volumes of reporter probe, capture probe, target probe, and hybridization-buffer (H-buffer) were added to solution with a consistent total working volume of 20 µL. The reporter and capture probe volumes created a molar ratio of 7.83×10^5. Varying volumes of the 100 µM synthetic target mRNA (target probe) was added to a H-buffer (SSC 5X, BSA 1%, and SDS 0.02%), along with reporter and capture probes in a microcentrifuge tube. Each target probe concentration was synthesized at 5 trials per concentration. These samples were incubated for 3

hours at 40 ℃ and 550 rpm on a thermal mixer with foil covering reactions. The final solutions were concentrated on a magnetic plate for separation. The pellets were washed 3 times with 2 μL of H-buffer. The final pellets were resuspended in 1 μL of the Ultrapure water and pipetted from the microcentrifuge tube onto a clean silicon wafer. This silicon wafer rested on a magnet, and the solution was pipetted up and down repeatedly to obtain a single pellet. This was characterized through Raman spectroscopy.

2.11 Whole Blood Lysis Protocol

Blood samples were obtained from ZenBio. For the lysis of the blood samples, 96 μL of QuantiGene™ lysis stock solution was added to a microcentrifuge tube and preheated for 30 minutes at 550 rpm and 37 ℃. 150 μL of Ultrapure RNAse free water and 6 μL of proteinase K solution were added to the lysis mixture along with 36 μL of whole blood. This solution was immediately vortexed for 1 minute and incubated for 1 hour at 550 rpm and 60 ℃. The lysis mixture was allowed to cool to room temperature before use.

2.12 Synthetic Pfs25-mRNA Target Hybridization in Lysed Blood

Hybridization in blood, similar to buffer, operated at a total working volume of 20 μL with a reporter to capture probe molar ratio of 7.83×10^5. The varying volumes of synthetic target mRNA probe was added to a microcentrifuge tube, along with reporter and capture probe volumes. The H-buffer volume was replaced with the blood lysate mixture. These samples were incubated for 3 hours at 40 ℃ and 550 rpm on a thermal mixer with foil covering reactions. The final solutions were concentrated on a magnetic plate for separation. The pellets were washed 1 time with 2 μL of H-buffer and moved to a new centrifuge tube to reduce any non-bound RP that

splashed on the walls of the tube. The pellets were washed 2 more times with 2 μL of H-buffer. The final pellets were resuspended in 1 μL of the Ultrapure water and pipetted from the microcentrifuge tube onto a clean silicon wafer. This silicon wafer rested on a magnet, and the solution was pipetted up and down repeatedly to obtain a single pellet. This was characterized through Raman spectroscopy.

2.13 SERS Characterizations using Horiba XploRA One™ Raman Microscope

The parameters for SERS measurements on hybridization samples using RB RP on silicon wafer are as follows: 10x objective lens, 638 nm laser operating on 25% power (~7 mW), grating 1200 (750 nm), hole: 500 μm, slit: 300 μm, 5 second acquisition time, 3 accumulations, and spectral range 800 – 1800 cm^{-1}. Per concentration, 5 replicates were performed and 1 measurement was obtained per replicate. Spectra were acquired and processed in LabSpec 6 software. Any further analysis of SERS spectra was completed in Igor Pro 8.

The parameters for SERS measurements on hybridization samples using Cy5 PEG RP on silicon wafer are as follows: 10x objective lens, 638 nm laser operating on 25% power (~7 mW), grating 1200 (750 nm), hole: 300 μm, slit: 100 μm, 10 second acquisition time, 1 accumulation, and spectral range 800 – 1800 cm^{-1}. Per concentration, 5 replicates were performed and 1 measurement was obtained per replicate. Spectra were acquired and processed in LabSpec 6 software. Any further analysis of SERS spectra was completed in Igor Pro 8.

The parameters for SERS measurements on hybridization samples using Cy7 PEG RP on silicon wafer are as follows: 10x objective lens, 785 nm laser operating on 25% power (~7 mW),

grating 1200 (750 nm), hole: 300 μm, slit: 100 μm, 5 second acquisition time, 3 accumulation, and spectral range 600 – 1600 cm^{-1}. Per concentration, 5 replicates were performed and 1 measurement was obtained per replicate. Spectra were acquired and processed in LabSpec 6 software. Any further analysis of SERS spectra was completed in Igor Pro 8.

2.14 DFS Characterizations using Cytoviva's Hyperspectral Microscope

7 μL of sample was drop casted onto a new glass slide with a coverslip over the sample. The sample dried for 24 hours to fix particles to glass slide and prevent oil leakage under coverslip. Spectral acquisition was performed using 60x oil immersion and the exposure time and size of scan for image acquisition determined based on intensity of sample being analyzed. Data was obtained and analyzed using ENVI 4.8 software.

CHAPTER 3: RESULTS AND DISCUSSION

3.1 Development of Rose Bengal SERS Substrate (RB Ag@AuNS)

We first developed the nucleic acid sandwich hybridization scheme to target Pfs25-mRNA with the rose bengal SERS substrate (RB Ag@AuNS) reporter probe (RP) to test the feasibility of the assay. This RP was nonresonant with the 638 nm laser used, allowing for little to no fluorescent background interference. Our hypothesis was that the nonresonant assay sensitivity would be decreased from the resonant assay sensitivity; however, the nonresonant assay would offer proof of concept as we would observe the RB RP characteristic peaks with no enhancement from fluorescence. This substrate experienced the SERS enhancement of a nanostar shape while also benefitting from the bimetallic structure. Due to this structure, the RB Raman tag was embedded between the layers at 60% surface saturation and did not experience complications due to competitive absorbance or surface variability. The RB Raman tag experiences an excitation peak at 559 nm, which is consistent with the UV/Vis spectrum in Figure 4. As expected, the SERS enhancement was an increased by a factor of 2 (Figure 4), which is comparably lower than Cy5, which experienced resonance Raman.

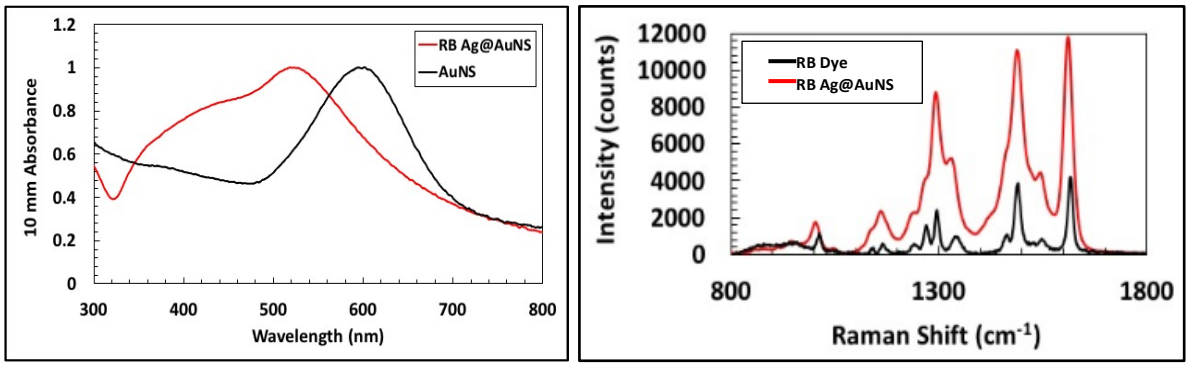

Figure 4. (Left) UV/Vis spectrum of AuNS in black and RB Ag@AuNS in red, experiencing a shift from 610nm to 529 nm. (Right) The SERS spectrum of the RB dye in black and the RB Ag@AuNS in red.

To further characterize the RB Ag@AuNS substrate, we utilized TEM. TEM was used as a characterization method to monitor the morphology and uniformity of the AuNS batch as well as the increase in size of the RB Ag@AuNS batch due to the attachment of the RB dye as well as the silver coating in the outer layer. The 638 nm AuNS TEM can be found below in Figure 5, confirming the success of the AuNS synthesis. The imageJ analysis displayed a 61.0 nm tip-to-tip length of the AuNS batch. The image obtained through TEM of the RB Ag@AuNS was analyzed to show a 120.3 nm size in tip-to-tip length. The growth in size combined with the visual cues in the TEM image exhibit a successful silver coating procedure. In total, TEM characterization proves the success in the AuNS synthesis and silver coating and, the wavelength shift in UV/Vis and SERS enhancement provided evidence of the success in the RB embedment. Overall, this displays a successful RB SERS substrate.

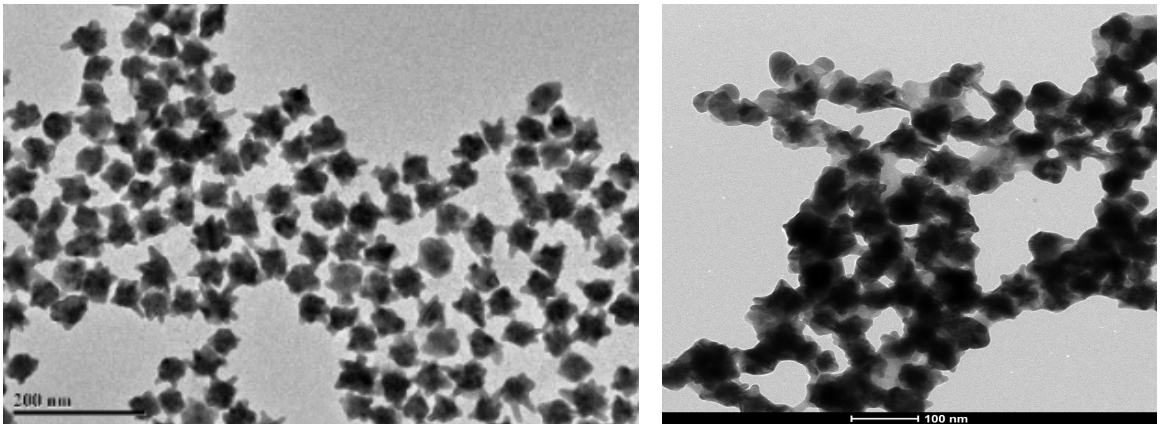

Figure 5. TEM images of (Left) 638 nm AuNSs and (Right) RB Ag@AuNS.

3.2 Development of Cyanine5 PEG SERS Substrate (Cy5 Ag@AuNS)

Next, we developed this nucleic acid sandwich hybridization scheme to target the Pfs25-mRNA biomarker again, but we replaced the RB RP with a cyanine5 SERS substrate (Cy5 Ag@AuNS) reporter probe (RP). We expanded the assay to the Cy5 RP to increase the sensitivity of the assay. The Cy5 RP was in resonance with the 638 nm laser used, allowing it to

experience an increase in sensitivity due to the fluorescence background. In similar fashion to the RB Ag@AuNS substrate, the Cy5 Ag@AuNS substrate was characterized via UV/Vis, TEM, and SERS. Figure 6 shows the UV/Vis, which shows the correct red shift needed to confirm the silver coating and binding of the Cy5 dye. The Cy5 Raman tag has an excitation peak at 651 nm. This study utilized a 638 nm laser, the Cy5 Raman tag experienced resonance Raman. The SERS enhancement increased by a factor of 10.8 (Figure 6).

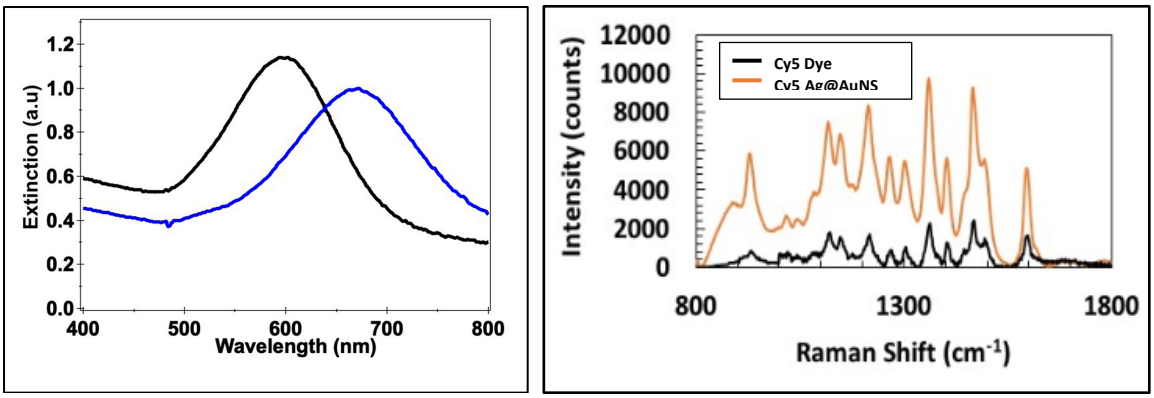

Figure 6. (Left) UV/Vis spectrum of AuNS in black and Cy5 Ag@AuNS in blue, experiencing a shift from 610nm to 652 nm. (Right) The SERS spectrum of the Cy5 dye in black and the

Figure 5 shows the success of the AuNS synthesis with a tip-to-tip length of 61.0 nm using imageJ. Figure 7 exhibits the TEM of the Cy5 Ag@AuNS substrate. After analysis, the tip-to-tip length was 122.5 nm. As experienced with the RB Ag@AuNS substrate, the size increase from 61.0 nm in the AuNS batch to 122.5 nm in the Cy5 Ag@AuNS batch verified the success of the silver coating onto the substrate, which is also visually observed in the TEM image. The UV/Vis confirmed the silver coating success with a shift toward the silver localized surface plasmon resonance (LSPR). The SERS spectrum displayed the success of the embedment of Cy5 dye between the outer silver coating and core shell gold nanostar.

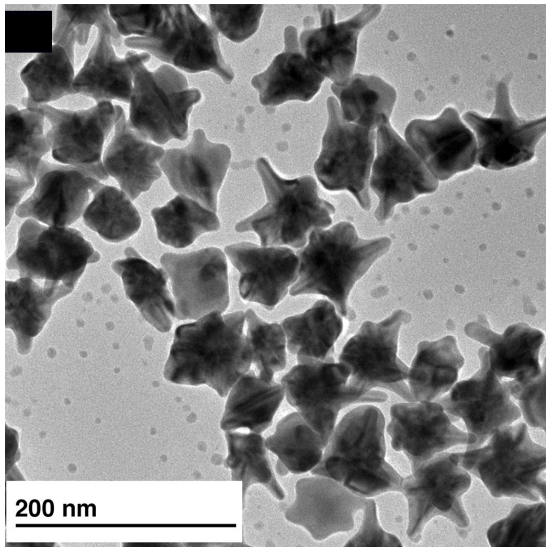

Figure 7. TEM image of Cy5 Ag@AuNS.

3.3 Development of Cyanine7 SERS Substrate (Cy7 Si@AuNS)

The final stage of this assay development was to complete the nucleic acid sandwich hybridization scheme again to target the Pfs25-mRNA biomarker using the cyanine7 SERS substrate (Cy7 Si@AuNS) reporter probe (RP). As our research lab possess a tabletop, research-grade Raman microscope with a 638 and 785 nm laser, we had to option to complete this assay in resonance with either laser. Our lab also possesses a 785 nm handheld Raman spectrometer. This assay was completed with the Cy7 RP as it was in resonance with the 785 nm laser, which was completed with the tabletop and handheld Raman instruments. This offered portability to our assay. The Cy7 Si@AuNS substrate was characterized through UV/Vis, TEM, and SERS. Figure 8 depicts the UV/Vis of the uncoated AuNS (black) and the Si@AuNS (blue). The blue shift from the uncoated AuNS at 704 nm to 788 nm once coated with silicon confirms the success of the coating step. Using a 785 nm laser, the Raman spectrum of the Cy7 dye (black) and the SERS spectrum of the Cy7 Si@AuNS RP (blue) is displayed in Figure 8. The SERS enhancement was a factor of 8.2. This is relatively closer to the enhancement of the Cy5

Ag@AuNS RP compared to the RB Ag@AuNS, which is theoretically in line with the resonance Raman that the Cy5 and Cy7 RPs experienced while the RB RP experienced nonresonance Raman.

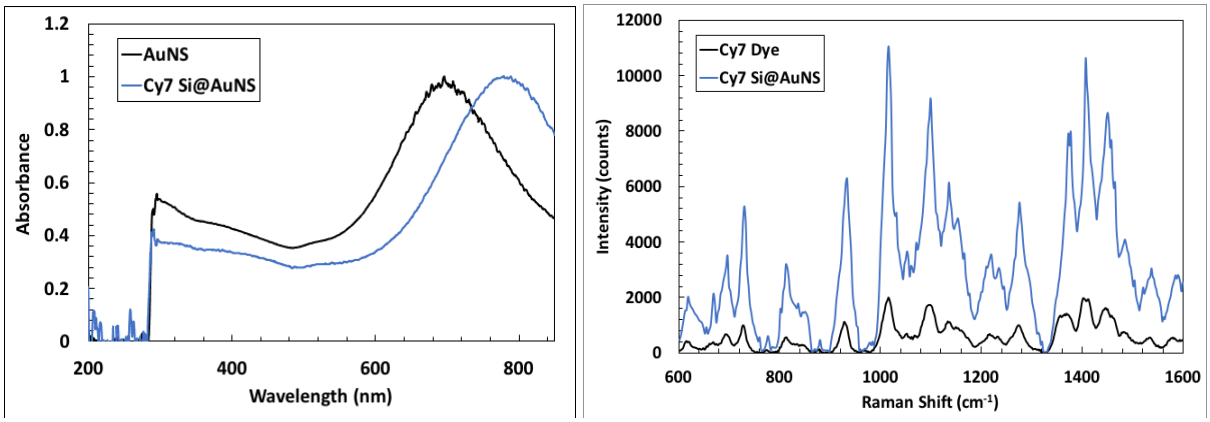

Figure 8. (Left) UV/Vis spectrum of AuNS in black and Cy7 Si@AuNS in blue, experiencing a shift from 704 nm to 788 nm. (Right) The SERS spectrum of the Cy7 dye in black and the Cy7 Si@AuNS in blue.

Figure 9 proves the success in the formation of AuNS (left) and the attachment of the Cy7 dye and silicon coating (right). This success is confirmed in the shift from a 251.94 nm tip-to-tip length in the uncoated AuNS to the 283.21 nm tip-to-tip length in the Cy7 Si@AuNS substrate, as analyzed by imageJ. This increase in size as well as the depiction of a clear silicon coating onto the AuNS in Figure 9 (left) shows the diameter of the silicon deposited. Overall, the UV/Vis shows a blue shift in wavelength, confirming the LSPR shift to silicon as well as to the excitation of Cy7 which is 756 nm.[53] The SERS spectra shows an enhancement in signal with the addition of the SERS substrate, and the TEM shows successful formation of the silicon coating and Cy7 embedment into the Cy7 Si@AuNS substrate.

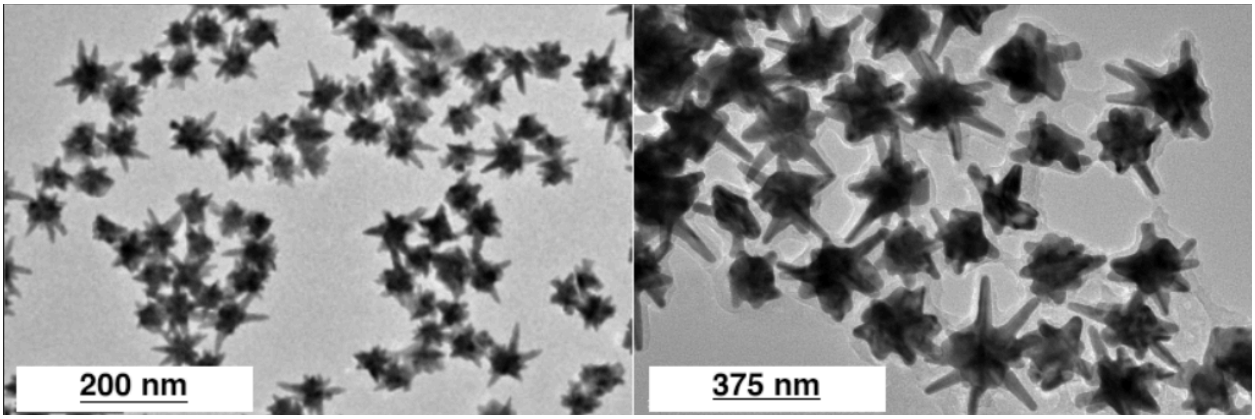

Figure 9. TEM images of (Left) AuNSs and (Right) Cy7 Si@AuNS.

3.4 Development of Silver Nanostar (AgNS) as an Alternative SERS Substrate

This assay currently utilizes a Ag@AuNS substrate, as there is ample research into the synthesis and reproduction of this silver-coated gold substrate composition. In this work, we also investigated the development of a novel Au@AgNS substrate. This substrate would benefit from the oxidation resistance that the outer gold layer would provide, which would call for a longer substrate shelf life. Since the nanostar would be composed of silver, this substrate would experience the enhanced optical scattering and absorbance properties silver provides. This would lead to a higher SERS enhancement and a more sensitive assay.

This work began with the protocol presented by Garcia-Leis et al.[47,48] The first trial of the AgNS synthesis followed by gold coating is depicted in the TEM image in Figure 8. The AgNS synthesis resulted in some branching, but the sample was nonuniform in size and shape. The gold coating of the same AgNS sample reduced branching, creating a sample of gold coated-silver nanoparticles.

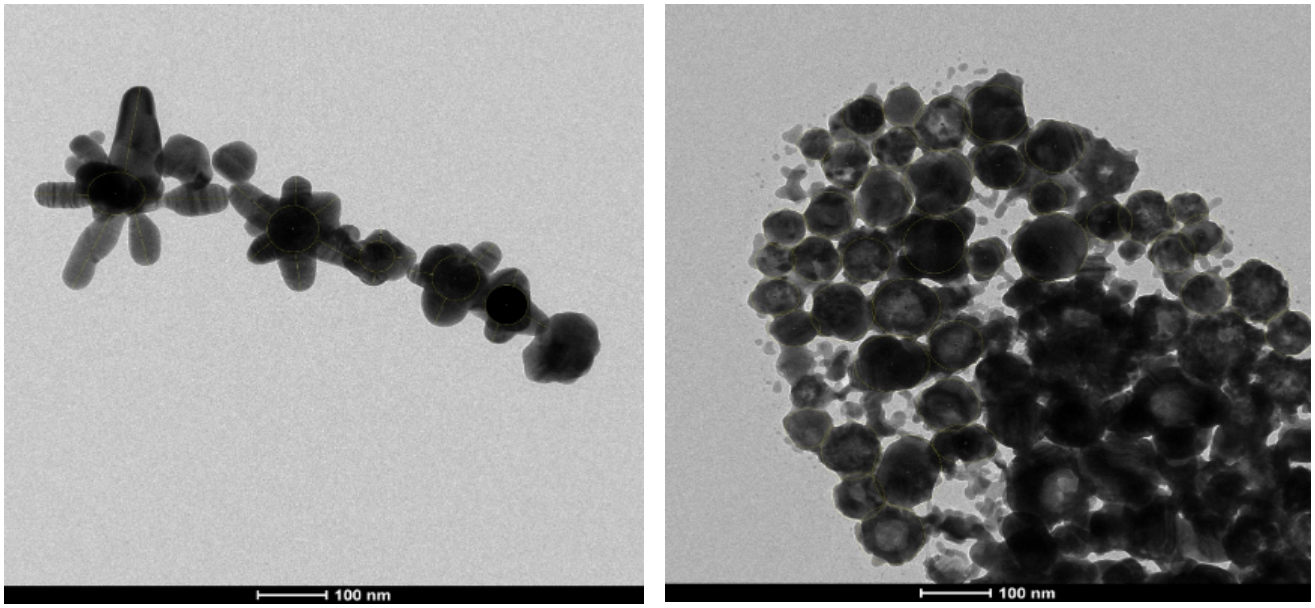

Figure 10. TEM images of (Left) AgNS and (Right) Au@AgNS.

The same methodology was used for AgNS synthesis, and a timed trial was developed to determine which mixing time would produce a uniform sample of AgNS. AgNSs were allowed to mix for 24, 48, 72, and 96 hours (Figure 9). The final step in the procedure was the addition of PEG for a surface coating.

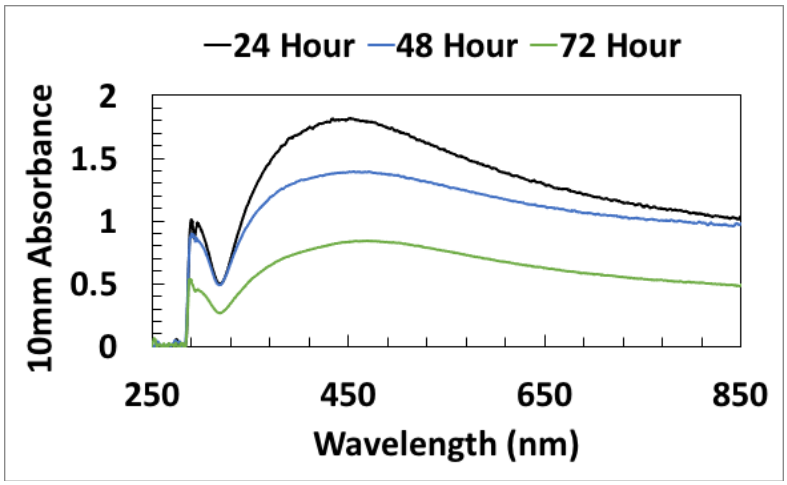

Figure 11. UV/Vis spectra of AgNS 24, 48, and 72 hour synthesis.

The 24, 48, and 72 hour syntheses progressed as expected with more precipitation in the solution at the higher mixing length. The 96 hour trial did not form a pellet after centrifugation,

and no UV/Vis data was viable from it. The UV/Vis spectrum shows a higher nanoparticle or nanostar production at the shortest mixing time. The spectrum also displayed a wavelength peak at 428 nm, which is consistent with the silver LSPR. The 24 hour trial's TEM image provided evidence for some branching, while the 48 hour trial did not.

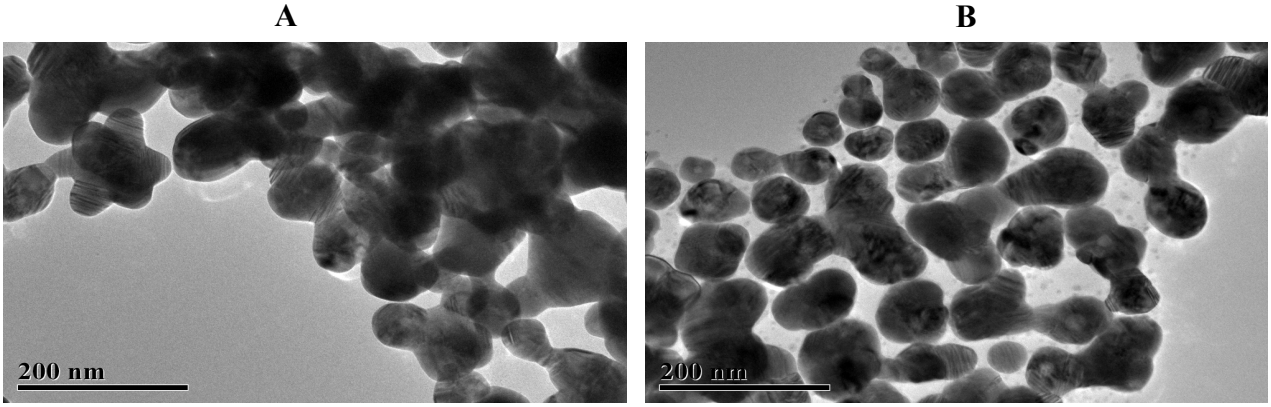

Figure 12. TEM image of AgNS (A) 24 and (B) 48 hour synthesis.

Based on the results of the time trials for the AgNS synthesis, the 24 hour mixing time was established for this synthesis. As shown in Figure 12, the 24 hour mixing time trial showed some branching, but we aimed to increase this branch length and uniformity to further increase SERS enhancement of this substrate. To do so, the citrate concentration was increased in the AgNS synthesis. Figure 13 contains the UV/Vis spectrum from this synthesis which contains a LSPR peak at 385 nm, in line with the LSPR for AgNSs. The image obtained via TEM proves the formation of a uniform batch of AgNS with successful branching (figure 13).

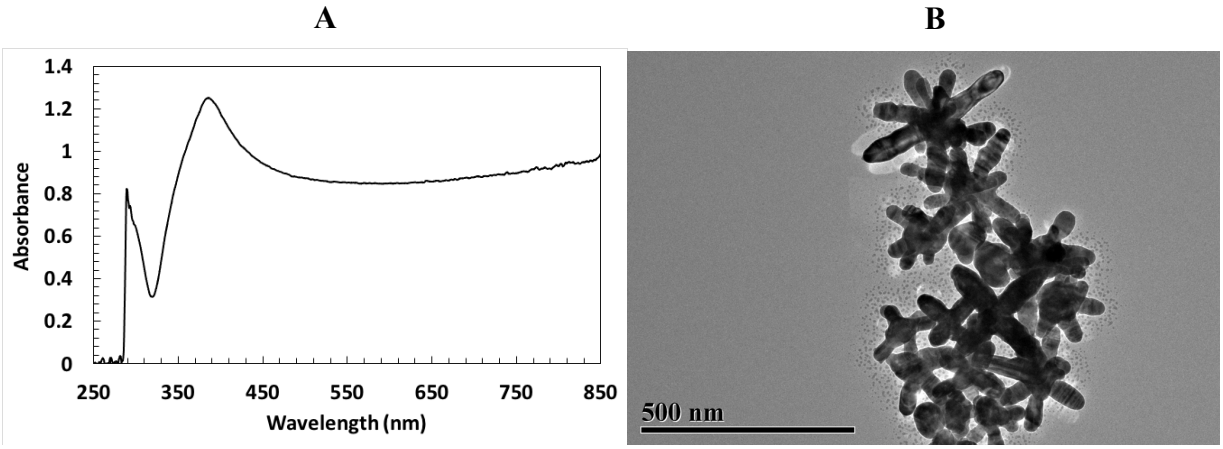

Figure 13. (A) UV/Vis spectrum and (B) TEM of AgNS after addition of increased citrate concentration during synthesis.

3.5 Optimized Reporter and Capture Probe Syntheses

Once the characterization of the RB, Cy5, and Cy7 substrates indicated the formation of AuNS, the embedment of the dye, and the success of the silver or silicon coating, the development reporter probe (RP) was the next phase of the assay, followed by the development capture probe (CP). The RP and CP sequences were developed to be partially complementary to the target synthetic malaria Pfs25-mRNA (TP) (Table 2). In order to withstand the hybridization protocol, the probe sequences were designed to have a melting temperature above 40 ºC and minimal secondary structures, as modeled by the IDT online platform. As seen in figure 11, this will allow the RPs and CPs to bind to separate ends of the target RNA. The surface saturation of these sequences onto the magnetic bead or SERS substrate was 60%. The CP magnetic beads were used for separation out of the biological matrix. The RP contained the SERS substrate which used the Raman tag as the signal reporter. The SERS enhancement of the RB RP was 2 orders of magnitude, as calculated from the intensity of the RB RP divided by the intensity of the RB dye at the 1489 cm^{-1} peak. The SERS enhancement of the Cy5 RP was 10 orders of magnitude, as calculated from the intensity of the Cy5 RP divided by the intensity of the Cy5 dye

at the 1360 cm^{-1} peak. The SERS enhancement of the Cy7 RP was 8 orders of magnitude, as calculated from the intensity of the Cy7 RP divided by the intensity of the Cy7 dye at the 1015 cm^{-1} peak. If the target RNA was not present in the solution, there would be no binding to join the RP and CP, and when the pellet was washed, the CP would be the only probe attached.

Table 2. Reporter Probe, Capture Probe, and Target Probe sequences, length, and melting temperatures.

Name	**Sequence**	**Length**	**Melting Temperature**
RP	5'-/ThiolMC6-D//iSp18//iSp18//iSp18/ AAA AAA AAA AAT GAA TAA ATT TTA-3'	24mer	42.9 ºC
CP	5'-GTT TGT TTC TTT TCC AAA AAA AAA AAA AAA/iSp18//iSp18//iSp18//3AzideN/-3'	30mer	51.5 ºC
TP	5'-GGA AAA GAA ACA AAC TGT AAA GTT TAT TCA T-3'	31mer	53.7 ºC

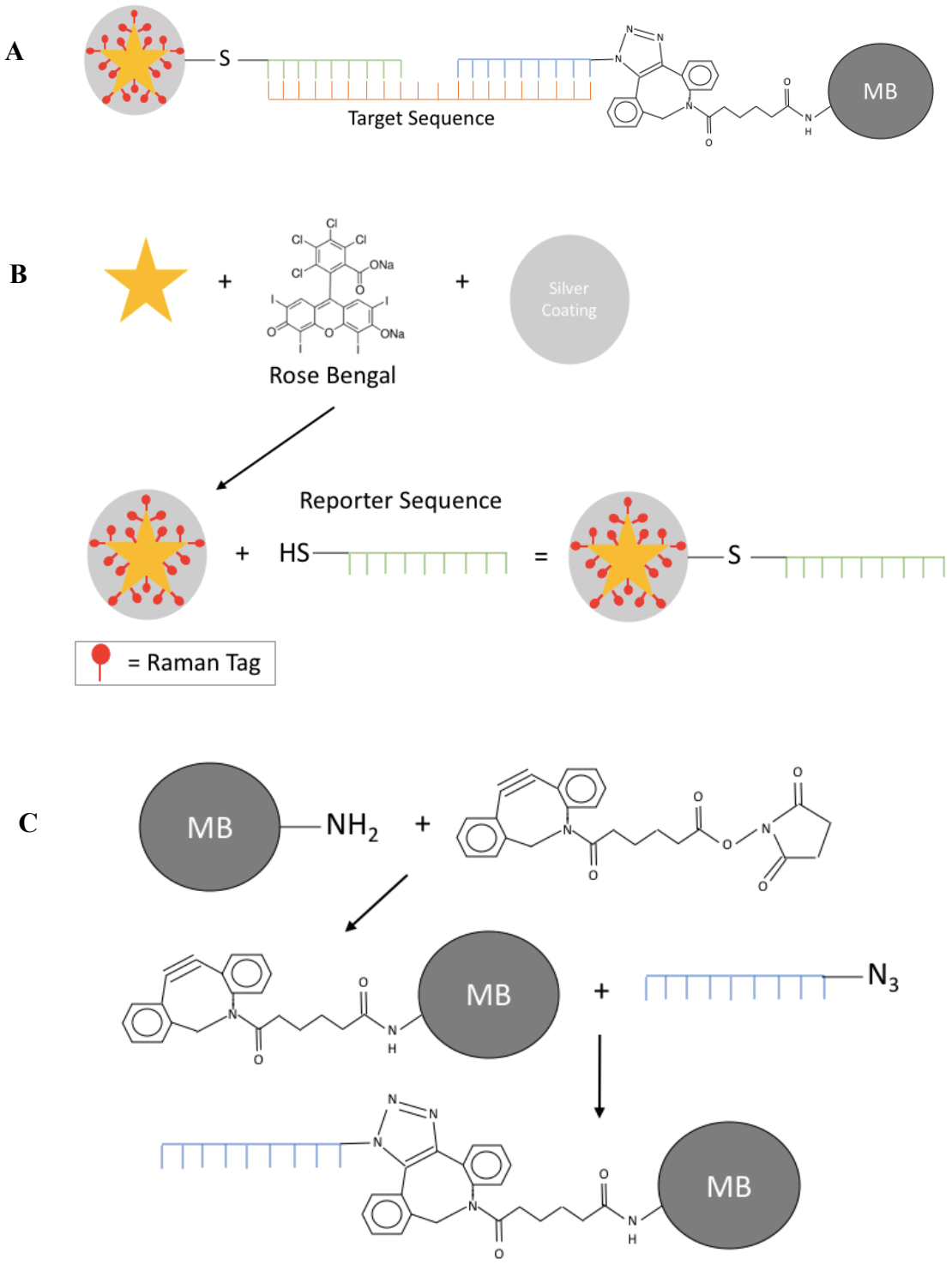

Figure 14. Hybridization schematic representation: (A) The entire hybridization complex containing the RP, CP, and target RNA. (B) The RP synthesis of SERS substrate with embedded Raman tag conjugated to the reporter sequence. (C) The CP synthesis with a magnetic bead attached to a DBCO-NHS linker to conjugate to the capture sequence.

3.6 Analytical Figures of Merit Calculations

Two analytical figures of merit were utilized to determine the sensitivity of this assay. The limit of detection (LOD) is classified as the lowest concentration that can be detected with the given system. The limit of quantification (LOQ) is the lowest concentration that can be detected with precision, leaving room for imprecision or bias. The LOD formula is (3.3 * standard deviation$_{intercept}$)/slope while the LOQ formula is (10 * standard deviation$_{intercept}$)/slope. The slope and intercept are associated with the concentration gradient to SERS intensity. To calculate the standard deviation and slope of the data points, a linear regression was performed in Excel.[49] The data points used in these calculations were the concentrations of the target within the hybridization complex. This will correlate to the concentration of parasite in patient blood when the assay is used for infected blood.

All tested target concentrations were plotted, and a Hill-Langmuir fitting was applied to the entire data set (Figures B2, C2, and C4). The inflection point of the fit was determined, to which a tangent line was applied. As the concentrations increased and created a plateau effect in the experimental curve, the difference in the tangent line to the Hill-Langmuir fitting becomes more pronounced. The length of the linear range of data points can be estimated based on the fit to this tangent line. This allowed for the determination of the linear dynamic range (LDR), which is the set of data points that follow a linear trend. These data points within this LDR were used for the LOD and LOQ calculations.[50, 51]

To determine the lowest concentration to attempt for the hybridization scheme, the signal to noise ratio was monitored, which is the intensity of a hybridization concentration at a characteristic peak divided by the intensity of the blank at that same peak. When the signal to noise ratio fell below 3, lower concentrations were not attempted.[49]

The relative standard deviation (RSD) was also calculated as the Cy5 RP was duplicated during the blood hybridization trials. The RSD is used to determine if the two RPs are similar enough to be considered reproducible. If the RSD is between 5 and 15% then the two RPs are considered reproducible, and it is feasible to use the data produced from these hybridizations together. The formula for the RSD is ((standard deviation*100)/average).[52]

3.7 Rose Bengal RP Hybridizations in Buffer

From the RB RP hybridization reaction data in hybridization buffer, a calibration curve was compiled (Figure 15). This calibration curve can be used to perform quantitative analysis for the biosensor in buffer. Each target probe concentration was synthesized with five replicates, with Raman analysis of 1 measurement per replicate. These measurements were acquired using the 638 nm laser excitation with an operating power of ~7 mW, as well as a 10x objective, 5 second acquisition time, and 3 accumulations per sample measurement. Standard deviation of each concentration was possibly influenced by the pellet formation onto the silicon wafer, any excess unwashed reporter probe solution left in microcentrifuge tube walls, or hybridization complex distribution in final pellet. The LDR was plotted as 8.3 to 83.3 nM, as determined by the Hill-Langmuir equation. The 1489 cm^{-1} characteristic RB peak was used for LOD calculations. The calculated LOD for the RB RP buffer assay was determined to be 15 nM or 9.0×10^9 RNA copies per microliter based on the hybridization reaction volumes of 20 µL. This converts to 7.2×10^6 gametocytes per microliter. The LOQ was determined to be 45 nM. These results indicated the successful detection of the Pfs25-mRNA biomarker in buffer hybridization reactions using the RB RP; however, this nonresonant Raman diagnostic method did not fall within the asymptomatic-stage detection window.

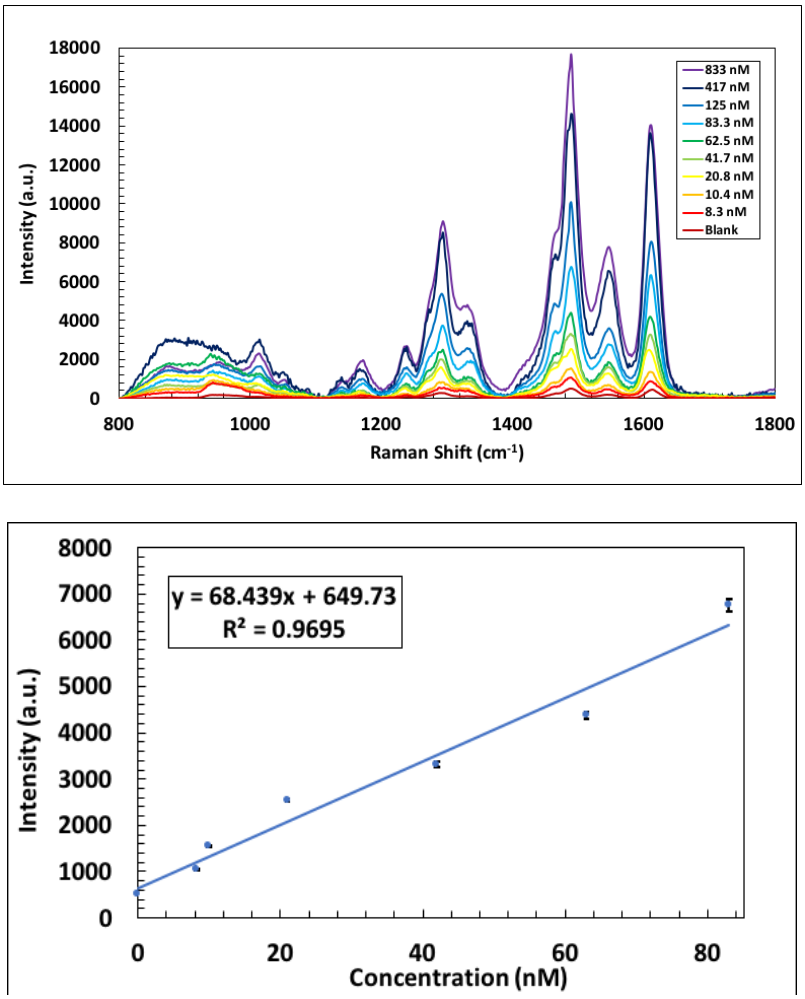

Figure 15. (Top) Average, stacked SERS spectra at each concentration of the RB RP LDR calibration curve, including the averaged blank signal. Blank samples are the use of the capture probe and reporter probe in the absence of the target during hybridization reactions. (Bottom) Pfs25-mRNA system in buffer calibration curve with RB RP with best fit and coefficient of determination for the linear range (8.3 nM to 83 nM).

3.8 Cyanine5 PEG RP Hybridizations in Buffer

From the Cy5 RP hybridization reaction data in H-buffer, a calibration curve was compiled (Figure 16). This calibration curve can be used to perform quantitative analysis for the biosensor in buffer. Each target probe concentration was synthesized with five replicates, with Raman analysis of 1 measurement per replicate. These measurements were acquired using the 638 nm laser excitation with an operating power of ~7 mW, as well as a 10x objective, 10 second acquisition time, and 1 accumulation per sample measurement. Standard deviation of each

concentration was possibly influenced by the pellet formation onto the silicon wafer, any excess unwashed reporter probe solution left in microcentrifuge tube walls, or hybridization complex distribution in final pellet.

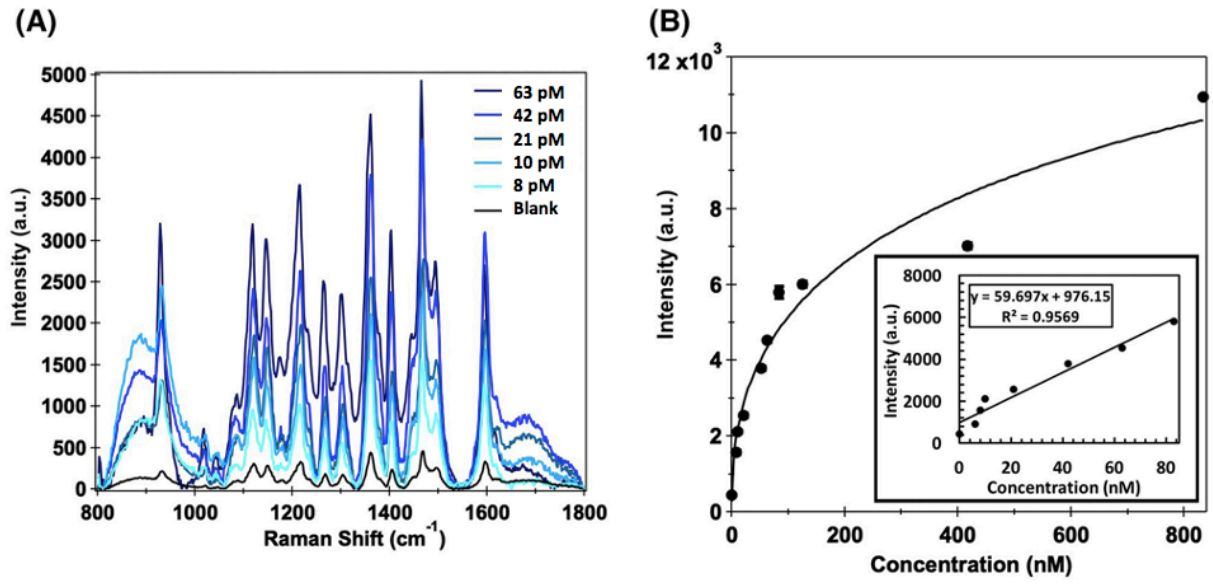

Figure 16. (A) Average, stacked SERS spectra at each concentration of the Cy5 RP in buffer LDR calibration curve, including the averaged blank signal. Blank samples are the use of the capture probe and reporter probe in the absence of the target during hybridization reactions. (B) Hill Langmuir fit with inset Pfs25-mRNA system in buffer calibration curve with Cy5 RP with best fit and coefficient of determination for the linear range (8.3 pM to 63 pM).

The LDR was plotted as 8.3 to 63 pM, as determined by the Hill-Langmuir equation. The 1360 cm^{-1} characteristic Cy5 peak was used for LOD calculations. The calculated LOD for the Cy5 RP buffer assay was determined to be 12 pM. The LOQ was determined to be 25 pM. These results indicated that the system can function in buffer down to picomolar concentrations. With the successful detection of the Pfs25-mRNA biomarker in buffer hybridization reactions using the Cy5 RP, the next step was to determine the functional ability of the assay using a synthetic target spiked-in blood lysate.

3.9 Cyanine5 PEG RP Hybridizations in Lysed Blood

In order to access the malaria RNA biomarker within the red blood cell, the whole blood samples needed to be lysed. Control measurements were performed on Cy5 reporter probe with lysed blood and capture probe with lysed blood. These three controls were tested using the same 638 nm laser excitation as done when using the buffer matrix. The control measurements for the lysed blood showed little to no signal at the Raman shift region of interest (1355 – 1365 cm^{-1}) which indicated no signal interference should occur due to the blood matrix. The Cy5 reporter probe in lysed blood produced the characteristic Cy5 SERS signal, indicating the observation of the 1360 cm^{-1} peak in the blood matrix. These controls were performed with no washing steps or purification steps.

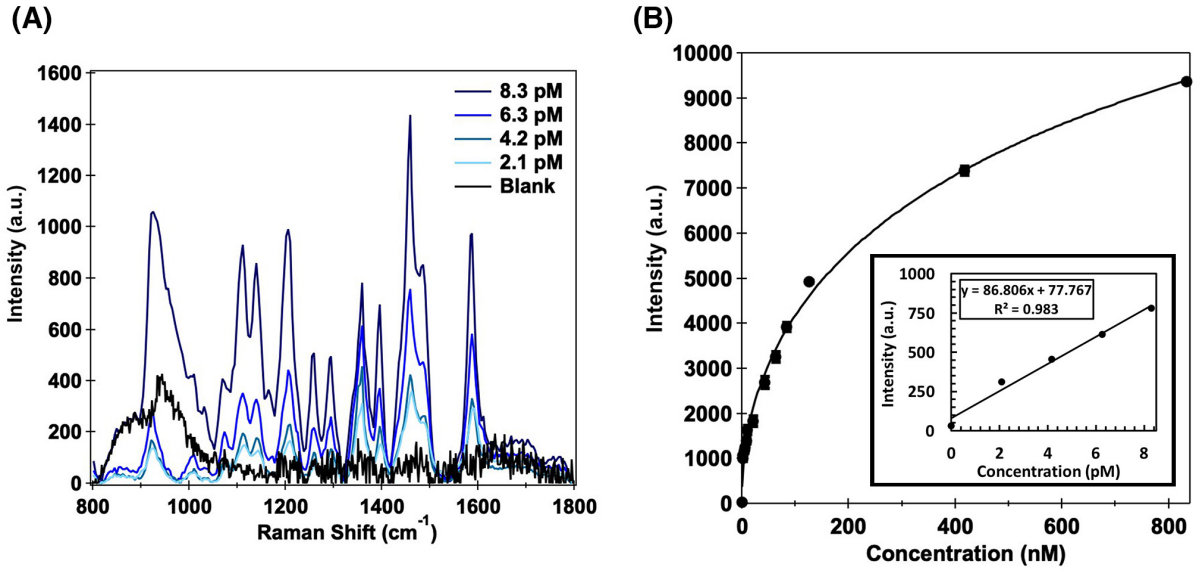

Figure 17. (A) Average, stacked SERS spectra at each concentration of the Cy5 RP in blood LDR calibration curve, including the averaged blank signal. Blank samples are the use of the capture probe and reporter probe in the absence of the target during hybridization reaction**. (**B) Hill Langmuir fit with inset Pfs25-mRNA system in blood calibration curve with Cy5 RP with best fit and coefficient of determination for the linear range (2.1 pM to 8.3 pM).

Each spectrum was 3rd degree polynomial background subtracted using the LabSpec6 software. After this background subtraction, the spectrum of each target probe concentration trial was compared to note the intensity change at the Cy5 Raman characteristic 1360 cm^{-1} peak. The individual spectrum at each target probe concentration can be found in Appendix C. This 1360 cm^{-1} peak was characteristic to the ν(C═V)ring stretch in the Cy5 structure. From this peak comparison, a calibration curve at the 1360 cm^{-1} peak was generated (Figure 17). This calibration curve plotted the LDR of the Cy5 blood assay, which was 2.1 to 8.3 pM. The LOD and LOQ calculations were performed using the same method as the buffer data. The calculated LOD for target spiked-in blood lysate was 1.3 pM or 7.7 x 10^5 RNA copies per µL reaction volume (Eq. 2). This translates to 2.5 x 10^3 gametocytes per µL reaction volume, as calculated in Equation 3.[27]

$$\text{RNA copies per } \mu L = \frac{(\text{ng/ } \mu L \text{ of DNA}) \times (6.022E23 \text{ mol}-1)}{(\text{Number of DNA nucleotides}) \times (325 \text{ g/mol}) \times (1E9 \text{ ng/g})} \quad \text{Eq. 2}$$

$$\text{Gametocytes per } \mu L = (10^{-1.6225}) \times (\text{RNA copies per } \mu L)^{0.8518} \quad \text{Eq. 3}$$

The LOQ for the blood hybridization reactions was 3.9 pM. The Cy5-PEG RP was replicated between the buffer and blood hybridization trials. To test reproducibility, the relative standard deviation at each overlapped concentration was calculated using the RSD percent. RSD values must fall between 5% to 15% for the replicates to be considered reproducible. The average RSD between the 2 Cy5-PEG RPs was 5%, with each overlapping concentration falling between the RSD range.

3.10 Cyanine7 PEG RP Hybridizations in Lysed Blood

In similar fashion to the Cy5 PEG RP, hybridizations in lysed blood were repeated using the Cy7 PEG RP. This transition to the Cy7 RP was done as the Cy7 RP is excited with a 785 nm laser, and the lab possesses a handheld Raman spectrometer with a 785 nm laser. This transition will allow the assay to be portable and will complete the final step of in-field application using this kit.

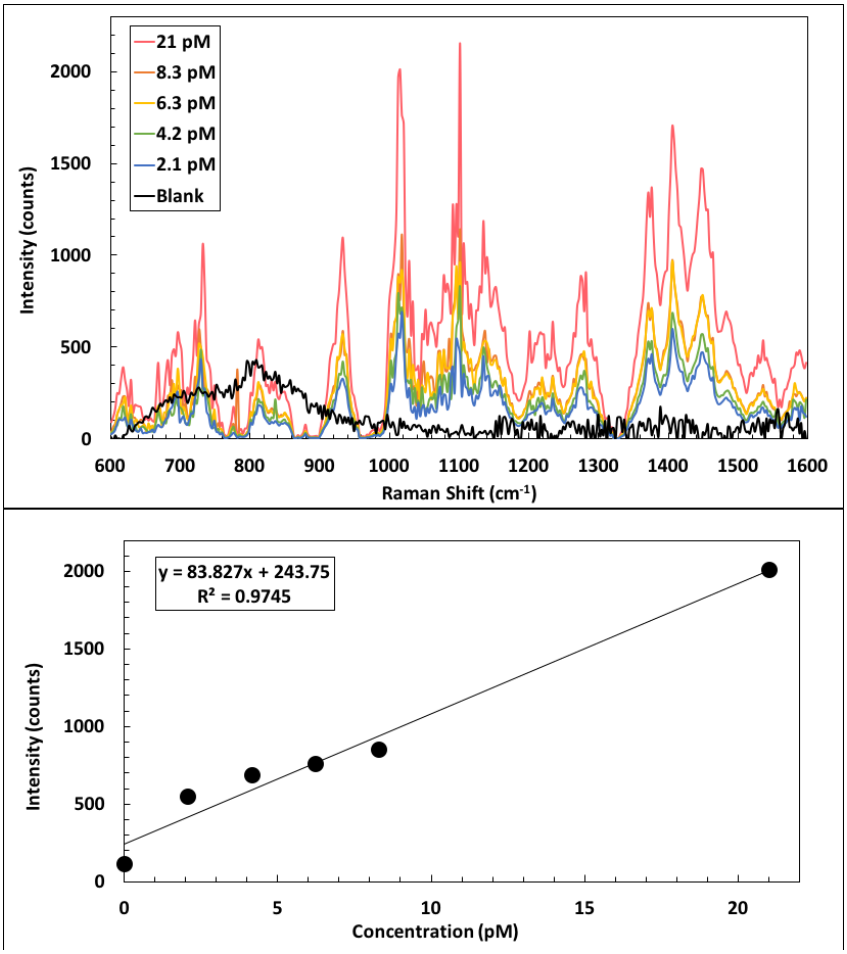

Figure 18. (Top) Average, stacked SERS spectra at each concentration of the Cy7 RP LDR calibration curve, including the averaged blank signal. Blank samples are the use of the capture probe and reporter probe in the absence of the target during hybridization reaction. (Bottom) Pfs25-mRNA system in blood calibration curve with Cy7 RP with best fit and coefficient of determination for the linear range (2.1 nM to 21 nM).

Figure 18 displays the overlapped SERS spectra of the LDR of the Cy7 RP hybridization in lysed blood with each spectrum 3rd degree polynomial background subtracted using the LabSpec6 software. The Cy7 characteristic 1015 cm^{-1} peak was used for intensity comparison as the concentrations of TP was changed and to calculate the overall LOD of this assay. Using this 1015 cm^{-1}, the calibration curve (Figure 18) was constructed for the LDR (2.1 to 21 pM), showing a proportional, linear increase in intensity with each concentration. This confirmed the success of the hybridization assay. The calculated LOD for target spiked-in blood lysate was 2.6 pM or 1.6 x 10^6 RNA copies based on 20 µL reaction volume. This translates to 4.5 x 10^3 gametocytes per 20 µL reaction volume. The LOQ for the blood hybridization reactions was 7.9 pM.

CHAPTER 4: CONCLUSIONS AND FUTURE WORK

4.1 Conclusions

This research serves as evidence that an indirect SERS-based platform for parasitic malaria RNA detection in the asymptomatic-stage is possible. This assay first utilized a Ag@AuNS SERS substrate for its electromagnetic SERS enhancement factors. The RB dye was first used as a Raman tag to test the feasibility of the assay. Once this was established and successful, the Cy5 dye was used as the Raman tag to increase the sensitivity of the assay. This is due to the utilization of a 638 nm laser to which the Cy5 was resonant to while the RB was nonresonant. Following this, the Cy7 dye was used as the Raman tag as it is in resonance with the 785 nm laser. Due to the availability of a 785 nm handheld Raman spectrometer, the Cy7 hybridization trials will afford portability for the assay.

The SERS intensity increase from the RB dye to the RB Ag@AuNS was on a 2 factor SERS enhancement factor, the SERS intensity increase from the Cy5 dye to the Cy5 Ag@AuNS was on a 10.8 factor SERS enhancement factor, and the SERS intensity increase from the Cy7 dye to the Cy7 Si@AuNS was on an 8.2 factor SERS enhancement factor. The LOD of the RB Ag@AuNS RP hybridization assay in buffer was 15 nM. The LOD of the Cy5 Ag@AuNS RP hybridization assay in buffer was 12 pM. The LOD of the Cy5 Ag@AuNS RP hybridization assay in blood was 1.3 pM. Based on calculations from Equations 2 and 3, a TP concentration of 1.3 pM is 7.7×10^5 RNA copies per µL reaction volume or 2.5×10^3 gametocytes per µL reaction volume. The LOD of the Cy7 Si@AuNS RP hybridization assay in blood was 2.6 pM. Based on calculations from Equations 2 and 3, a TP concentration of 2.6pM is 1.6×10^6 RNA copies per µL reaction volume or 4.5×10^3 gametocytes per µL reaction volume. Overall, this shows that the resonance Raman trials of Cy5 and Cy7 hybridization in lysed blood fall close in sensitivity

while being more sensitive than the nonresonance Raman RB hybridizations. With both Cy5 and Cy7 hybridization assays in blood falling below 10^4 gametocytes per microliter, this classifies this resonant Raman assay as capable of detection in the asymptomatic-window.

4.2 Optimizing SERS Substrate using Silver Nanostars (AgNS)

As stated, this thesis includes the development of a Ag@AuNS substrate. This novel substrate type will benefit from the optical properties of silver as it is the bulk of the substrate in the nanostar core-shell form. It will also have oxidation resistance, as the outer layer is gold. This resistance will lead to a longer substrate self-life. The LSPR of the substrate will be able to exceed 500 nm, as gold possesses a higher LSPR than silver. Due to this, Raman tags with LSPRs in the 700 to 800 nm range can be used and retain their high LSPR to be in resonance with the 785 nm laser. We aim to achieve a higher SERS enhancement with this new substrate as well as a longer shelf life, which will be advantageous for point of care (POC) application in resource-limited areas.

The priority of this Au@AgNS substrate development is to achieve a uniform batch of AgNS with a high degree of branching as it will increase the SERS enhancement of the substrate. Current UV/Vis data supports more silver nanostar production with a 24 hour mixing time. Images obtained through TEM provide evidence that the combination of a 24 hour mixing time with increased citrate concentration for a higher reduction yields an optimal, uniform batch of highly branched AgNS. For future work, our aim is to develop a novel protocol for the gold coating of the AgNS. Once this synthesis is established, we will attempt to embed a Raman tag between these bimetallic layers and compare the SERS enhancement achieved to our current Ag@AuNS substrate.

4.3 Transition to Portable Handheld Raman Spectrometer

The nucleic acid sandwich hybridization assay to target the malaria parasitic Pfs25-mRNA in the asymptomatic concentration range began with the use of RB as the Raman tag. This substrate was nonresonant with the 638 nm laser, but it was initially used to test the proof of concept of the assay as it experienced no interference from fluorescent background. Once this first phase was complete, the assay was repeated utilizing the Cy5 Raman tag. The Cy5 Raman tag was in resonance with the 638 nm laser. This resonance Raman mode allowed for a larger SERS enhancement factor, and this Cy5 RP hybridization system experienced a lower sensitivity. Next, the Cy7 Raman dye was used as it is in resonance Raman mode with the 785 nm laser. With the availability of a 785 nm handheld Raman spectrometer, this will allow the assay to be portable which will aid in in-field applications. Our overall goal is to adapt the work reported here into a POC applicable, portable SERS-based biosensor that can be utilized in resource-limited areas as an inexpensive, time-efficient malaria diagnostic tool.

Since the Cy7 Si@AuNS hybridization in lysed blood has been completed with the tabletop, research-grade Raman microscope, the next stage is to complete comparisons with the handheld Raman spectrometer. To do this, the LDR of the Cy7 hybridizations in lysed blood will be redone and measured using both the tabletop and handheld Raman spectrometers. The signal acquisition will be compared as well as the intensity of the characteristic 1015 cm^{-1} peak. If these measurements are comparable, the comparison of the 3 dyes in this work will be finalized.

4.4 Finalization of Assay through Integrated, Field-Applicable Platform

We aim to combine our biosensor into an integrated, portable platform. This platform will combine the RP, CP, TP hybridization scheme in a field applicable format with the use of our handheld Raman spectrometer. This combination will increase the portability of our assay, and this assay can be tested in-field. We plan to explore the concept of a capture probe consisting of AuNPs conjugated to a glass capillary tube. The previously used CP complimentary DNA strand will be attached to the AuNPs per the usual DBCO synthesis. This stick will be dipped into a vial with RP and the target RNA. Once this hybridization solution has incubated, the capture probe stick could be pulled from the solution, bringing the target RNA and bound RP with it. This would allow for easier washing steps, as the stick could be dipped into or sprayed by the buffer and water. Overall, this would allow for an easier POC application as it removes the need for micro-pipetting.

Another venture that would allow for an enhanced integrated system is a thresholding software program. We aim to engineer a software program that will filter the data uploaded from a measurement taken on the handheld Raman. This software would then focus on the intensity at a specified characteristic peak. We would reference our infected blood calibration curve as to what our LOD would be. The software would threshold at this LOD concentration and respond with a “yes” for any intensity above the LOD and give a “no” for intensities lower than this. Our aim is to have a system that would give a simple binary answer as the malaria diagnosis for time efficiency and user-friendliness. Our combination of an optimized SERS substrate, well-developed CP, handheld Raman use, and thresholding software program will allow our SERS-based biosensor to detect malaria in its early, asymptomatic-stage with time efficiency, portability, and sensitivity.

REFERENCES

1. Organization, WHO. https://www.who.int/news-room/fact-sheets/detail/malaria
2. Vale, N.; Aguiar, L.; Gomes, P. Antimicrobial peptides: a new class of antimalaria drugs? *Front. Pharmacol*. **2014**, 5 (275), 1-13.
3. Organization, The Jenner Institute. https://www.jenner.ac.uk/about/resources/about-malaria
4. Tuteja, R. Malaria – an overview. *The FEBS Journal*. **2007**, 274 (18), 4670-4679.
5. Hathiwala, R.; Mehta, P.R.; Nataraj, G.; Hathiwala, S. LED fluorescence microscopy: Novel method for malaria diagnosis compared with routine methods. *J. Infect. Public Health*. **2017**, 10 (6), 824-828.
6. Organization, CDC. https://www.cdc.gov/malaria/diagnosis_treatment/diagnostic_tools.html
7. Recht, J.; Siqueira, A.M.; Monteiro, W.M.; Herrera, S.M.; Herrera, S.; Lacerda, M.V.G. Malaria in Brazil, Colombia, Peri and Venezuela: current challenges in malaria control and elimination. Malar. J. 2017, 16 (273).
8. Wilson, M. L. Malaria Rapid Diagnostic Tests. *Clinical Infectious Diseases.* **2012**, 54 (11), 1637-1641.
9. Johnston, S.P.; Pieniazek, N.J.; Xayavong, M.V.; Slemenda, S.B.; Wilkins, P.P.; da Silva, A.J. PCR as a Confirmatory Technique for Laboratory Diagnosis of Malaria. *J. Clin. Microbiol*. **2005**, 44 (3), 1087-1089.
10. Chang, D.; Tram, K.; Li, B.; Feng, Q.; Shen, Z.; Hee, C.H.; Salena, B.J.; Li, Y. Detection of DNA Amplicons of Polymerase Chain Reaction Using Litmus Test. *Sci. Rep.* **2017**, 7 (3110).
11. Ziegler, C.; Göpel, W. Biosensor Development. *Curr. Opin. Chem. Biol*. **1998,** 2 (5), 585-591.
12. Davis, J.; Vaughan, D.H.; Cardosi, M.F. Elements of biosensor construction. *Enzyme Microb. Technol.* **1995,** 17 (12), 1030-1035.
13. Poon, L.L.M.; Wong, B.W.Y.; Ma, E.H.T.; Chan, K.H.; Chow, L.M.C.; Abeyewickreme, W.; Tangpukdee, N.; Yuen, K.Y.; Guan, Y.; Looareesuwan, S.; Malik Peiris, J.S. Sensitive and Inexpensive Molecular Test for Falciparum Malaria: Detecting *Plasmodium falciparum* DNA Directly from Heat-Treated Blood by Loop-Mediated Isothermal Amplification. *Clinical Chemistry.* **2006,** 52 (2), 303-306.
14. Barhoumi, A.; Halas, N. Label-Free Detection of DNA Hybridization Using Surface Enhanced Raman Spectroscopy. *J. Am. Chem. Soc*. **2010**, 132 (37), 12792-12793.
15. Ranki, M.; Palva, A.; Virtanen, M.; Laaksonen, M.; Soderlund, H. Sandwich hybridization as a convenient method for the detection of nucleic acids in crude samples. *Gene*. **1983**, 21 (1-2), 77-85.
16. Ngo, H.T.; Gandra, N.; Fales, A.M.; Taylor, S.M.; Vo-Dinh, T. Sensitive DNA detection and SNP discrimination using ultrabright SERS nanorattles and magnetic beads for malaria diagnostics. *Biosens. Bioelectron.* **2016**, 81 (15), 8-14.
17. Wampfler, R.; Mwingira, F.; Javati, S.; Robinson, L.; Betuela, I.; Siba, P.; Beck, H.; Mueller, I.; Felger, I. Strategies for Detection of Plasmodium species Gametocytes. *PLOS One*. **2013**, 8 (9).
18. Galatas, B.; Bassat, Q.; Mayor, A. Malaria Parasites in the Asymptomatic: Looking for the Hay in the Haystack. *Trends Parasitol.* **2016**, 32 (4), 296-308.

19. Scally, S.W.; McLeod, B.; Bosch, A. Molecular definition of multiple sites of antibody inhibition of malaria transmission-blocking vaccine antigen Pfs25. *Nat. Commun.* **2017**, 8 (1568).
20. Organization, ACS. https://www.acs.org/content/acs/en/education/whatischemistry/landmarks/ramaneffect.html
21. Mulvaney, S.P.; Keating, C.D. Raman Spectroscopy. *Anal. Chem*. **2000**, 72 (12), 145-158.
22. Wang, X.; Huang, S.C.; Hu, S.; Yan, S.; Ren, B. Fundamental understanding and applications of plasmon-enhanced Raman spectroscopy. *Nat. Rev. Phys.* **2020**, 2, 253-271.
23. Stiles, P.L.; Dieringer, J.A.; Shah, N.C.; Van Duyne, R.P. Surface-Enhanced Raman Spectroscopy. *Annu. Rev. Anal. Chem.* **2008**, 1, 601-626.
24. Tian, Z.Q. Surface-enhanced Raman spectroscopy: advancements and applications. *J. Raman Spectrosc.* **2005**, 36 (6-7), 466-470.
25. Le Ru, E.C.; Meyer, M.; Blackie, E.; Etchegoin, P.G. Advanced aspects of electromagnetic SERS enhancement factors at a hot spot. *J. Raman Spectrosc.* **2008**, 39 (9), 1127-1134.
26. He, S.; Chua, J.; Tan, E.K.M.; Kah, J.C.Y. Optimizing the SERS enhancement of a facile gold nanostar immobilized paper-based SERS substrate. *RSC Adv.* **2017,** (27).
27. Hamm, L.; Gee, A.; De Silva Indrasekara, A.S. Recent Advancement in the Surface-Enhanced Raman Spectroscopy-Based Biosensors for Infectious Disease Diagnosis. *Appl. Sci.* **2019,** 9 (7), 1448.
28. Zhang, L.; Li, X.; Hao, R.; Jia, H.; Dai, Y.; Amin, M.U.; You, H.; Li, T.; Fang, J. Highly active Au NP microarray films for direct SERS detection. *J. Mater. Chem. C.* **2019**, 48.
29. Cao, Y.C.; Jin, R.; Mirkin, C.A. Nanoparticles with Raman Spectroscopic Fingerprints for DNA and RNA Detection. *Science.* **2002**, 297 (5586), 1536-1540.
30. Chen, F.; Flaherty, B.R.; Cohen, C.E.; Peterson, D.S.; Zhao, Y. Direct detection of malaria infected red blood cells by surface enhanced Raman spectroscopy. *Nanomedicine: NBM.* **2016,** 12 (6), 1445-1451.
31. Yuen, C.; Liu, Q. Magnetic field enriched surface enhanced resonance Raman spectroscopy for early malaria diagnosis. *J. of Biomedical Optics.* **2012,** 17 (1).
32. Mhlanga, N.; Domfe, T.; Skepu, A.; Netho, T.A. Sandwich-based surface-enhanced Raman scattering probes for detection and quantification of malaria. *J. Raman Spectrosc.* **2020**, 51 (12), 2416-2424.
33. Maier, Stefan Alexander. Plasmonics: Fundamentals and Applications. New York, Springer Science and Business Media LLC, **2007**.
34. Marinakos, S.M.; Chen, S.; Chilkoti, A. Plasmonic Detection of a Model Analyte in Serum by a Gold Nanorod Sensor. *Anal. Chem.* **2007**, 79 (14), 5278-5283.
35. Das, C.M.; Guo, Y.; Kang, L.; Ho, H.; Yong, K.T. Investigation of Plasmonic Detection of Human Respiratory Virus. *Adv. Theory Simul.* **2020**, 3 (7).
36. Borinskina, S.V.; Ghasemi, H.; Chen, G. Plasmonic materials for energy: From physics to applications. *Mater. Today.* **2013,** 16 (10), 375-386.
37. Gutiérrez, Y.; Brown, A.S.; Moreno, F.; Losurdo, M. Plasmonics beyond noble metals: Exploiting phase and compositional changes for manipulating plasmonic performane. *J. Appl. Phys.* **2020**, 128.

38. Dormeny, A.A.; Sohi, P.A.; Kahrizi, M. Design and simulation f a refractive index sensor based on SPR and LSPR using gold nanostructures. *Results Phys.* **2020**, 16.
39. Origanization, Nicoya. https://nicoyalife.com/nicoya-surface-plasmon-resonance-resources/what-is-spr/lspr-vs-spr-2/#:~:text=Although%20SPR%20sensors%20have%20a,biomolecular%20binding%20events%20is%20similar.&text=This%20smaller%20sensing%20volume%20means,less%20sensitive%20to%20bulk%20effects.
40. Gong, C.; Leite, M.S. Noble Metal Alloys for Plasmonics. *ACS Photonics.* **2016,** 3 (4), 507-513.
41. Doria, G.; Conde, J,; Veigas, B.; Giestas, L.; Almeida, C.; Assunção, M.; Rosa, J.; Baptista, P.V. Noble Metal Nanoparticles for Biosensing Applications. *Sensors.* **2012,** 12 (2), 1657-1687.
42. Rasmagin, S.I.; Apresyan, L.A. Analysis of the Optical Properties of Silver Nanoparticles. *Opt. Spectrosc.* **2020,** 128, 327-330.
43. Rycenga, M.; Cobley, C.M., Zeng, J.; Li, W.; Moran, C.H.; Zhang, Q.; Win, D.; Xie, Y. Controlling the Synthesis and Assembly of Silver Nanostructures for Plasmonic Applications. *Chem. Rev.* **2011,** 111 (6), 3669-3712.
44. Organization, ThoughtCo. https://www.thoughtco.com/introduction-to-noble-metals-608444#:~:text=According%20to%20this%20definition%2C%20gold,ruthenium%2C%20osmium%2C%20and%20iridium.
45. Li, J. F.; Zhang, Y. J.; Ding, S. Y.; Panneerselvam, R.; Tian, Z. Q., Core-Shell Nanoparticle-Enhanced Raman Spectroscopy. *Chemical Reviews* **2017**; 117 (7), 5002-5069.
46. Unser, S.; Bruzas, I.; He, J.; Sagle, L. Localized Surface Plasmon Resonance Biosending: Current Challenges and Approaches. *Sensors.* **2015**, 15 (7), 15684-15716.
47. Doering, W. E.; Nie, S. Spectroscopic Tags Using Dye-Embedded Nanoparticles and Surface-Enhanced Raman Scattering. *Anal. Chem.* **2003**; 75 (22), 6171-6176.
48. Garcia-Leis, A.; Rivera-Arreba, I.; Sanchez-Cortes, S., Morphological tuning of plasmonic silver nanostars by controlling the nanoparticle growth mechanism: Application in the SERS detection of the amyloid marker Congo Red. *Colloids and Surfaces a-Physicochemical and Engineering Aspects* **2017**; 535, 49-60.
49. Lavin, A.; De Vincente, J.; Holgado, M.; Laguna, M.F.; Casquel, R.; Santamaría, B.; Maigler M.V.; Hernández, A.L.; Ramírez, Y. On the Determination of Uncertainty and Limit of Detection in Label-Free Biosensors. *Sensors.* **2018,** 18 (7), 2038.
50. Borisov, I.A.; Lobanov, A.V.; Reshetilov, A.N.; Kurganov, B.I. Quantitative Analysis of the Calibration Dependences for Biosensors. *Appl. Biochem. Microbiol.* **2000,** 36 (3), 215-220.
51. Kurganov, B.I.; Lobanov, A.V.; Borisov, I.A.; Reshetilov, A.N. Criterion for Hill equation validity for description of biosensor calibration curves. *Anal. Chim. Acta.* **2001,** 427 (1), 11-19.
52. Gauglitz, G. Analytical evaluation of sensor measurements. *Anal. Bioanal. Chem.* **2018,** 410, 5-13.
53. AAT Bioquest. https://www.aatbio.com/fluorescence-excitation-emission-spectrum-graph-viewer/cy7_cyanine_7#:~:text=Cy7%20(Cyanine%2D7)%20is,emission%20peak%20at%20779%20nm.

SUPPLEMENTAL INFORMATION

APPENDIX A – Gold Nanoparticles for Seed-mediated AuNS Growth

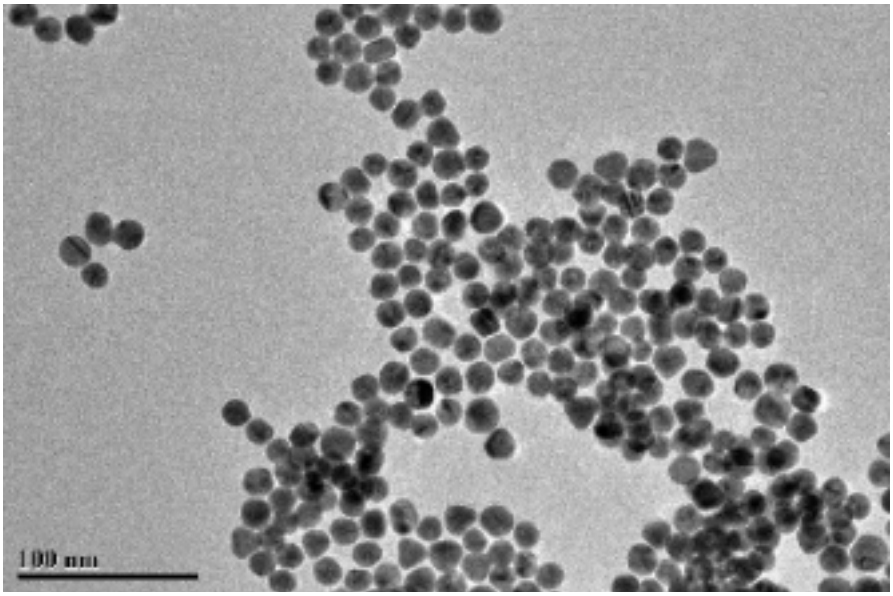

Figure A1. TEM of 15 nm spherical gold nanoparticles (AuNP) used for AuNS synthesis.

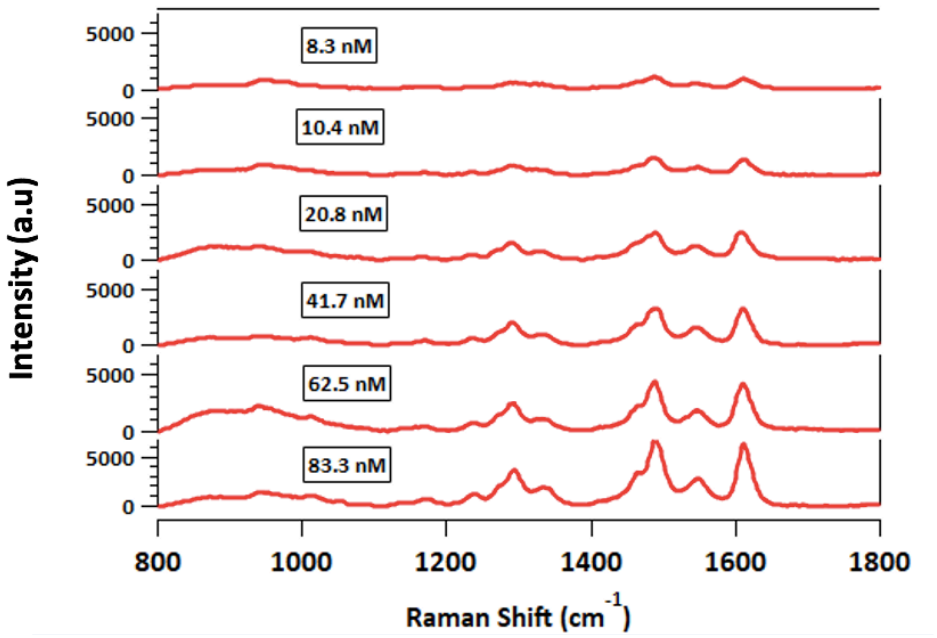

Figure B1. Stacked SERS spectra of RBRP **buffer** hybridizations at concentrations within LDR.

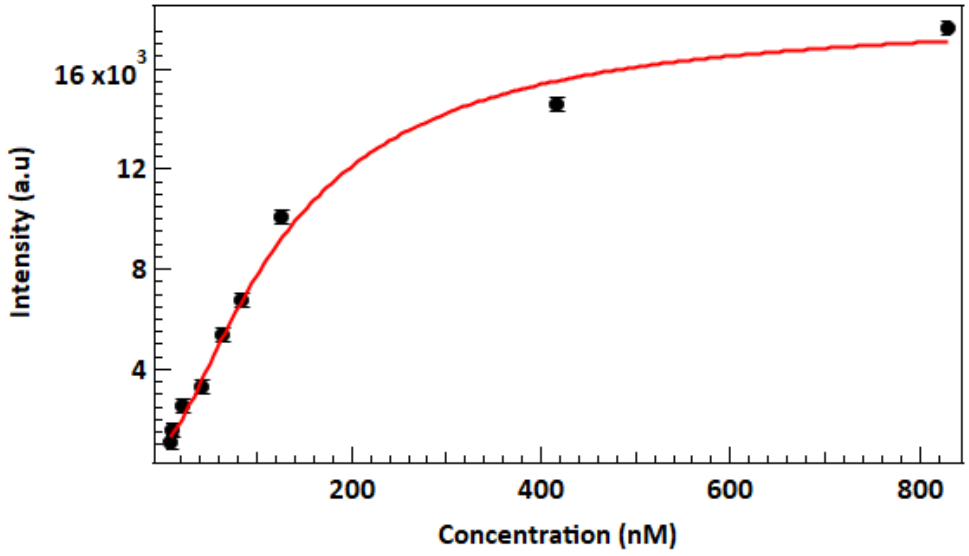

Figure B2. Hill-Langmuir fitting over entire range of concentrations tested in RB RP **buffer** hybridizations. LDR determined from tangent line at inflection point of Hill-Langmuir fit.

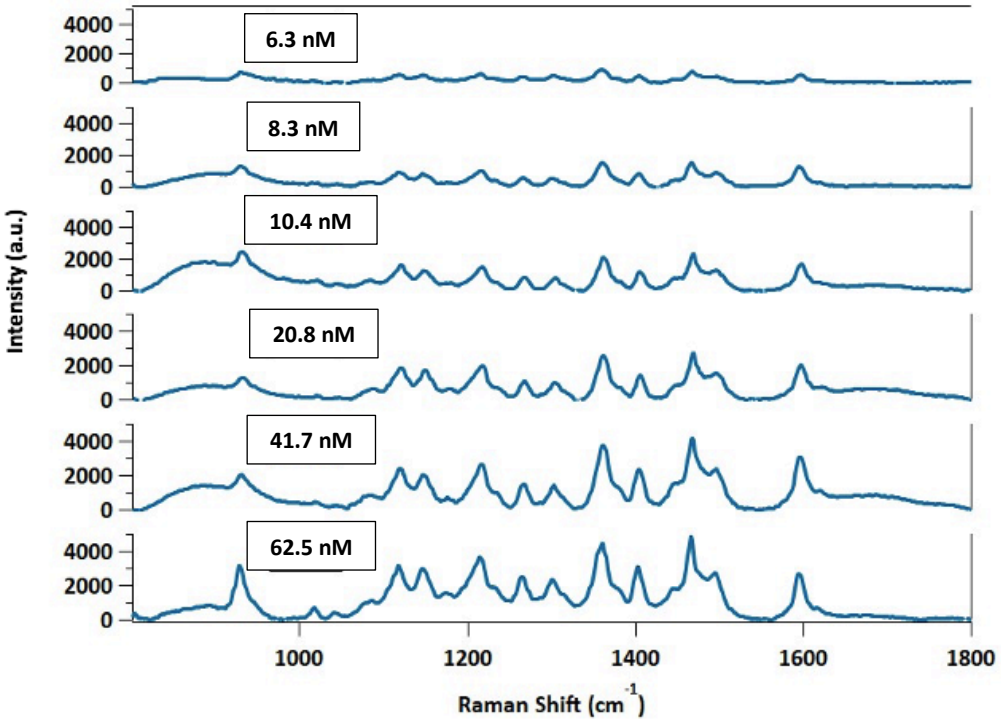

Figure C1. Stacked SERS spectra of Cy5 PEG RP **buffer** hybridizations at concentrations within LDR.

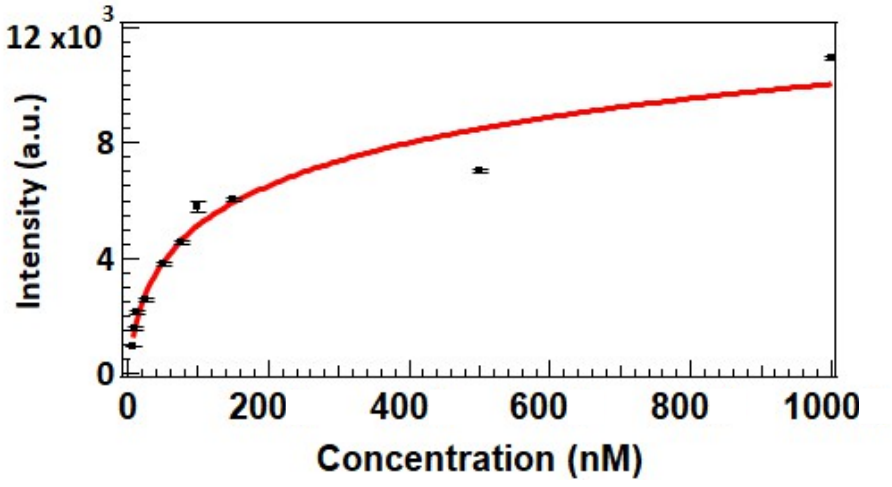

Figure C2. Hill-Langmuir fitting over entire range of concentrations tested in Cy5 RP **buffer** hybridizations. LDR determined from tangent line at inflection point of Hill-Langmuir fit.

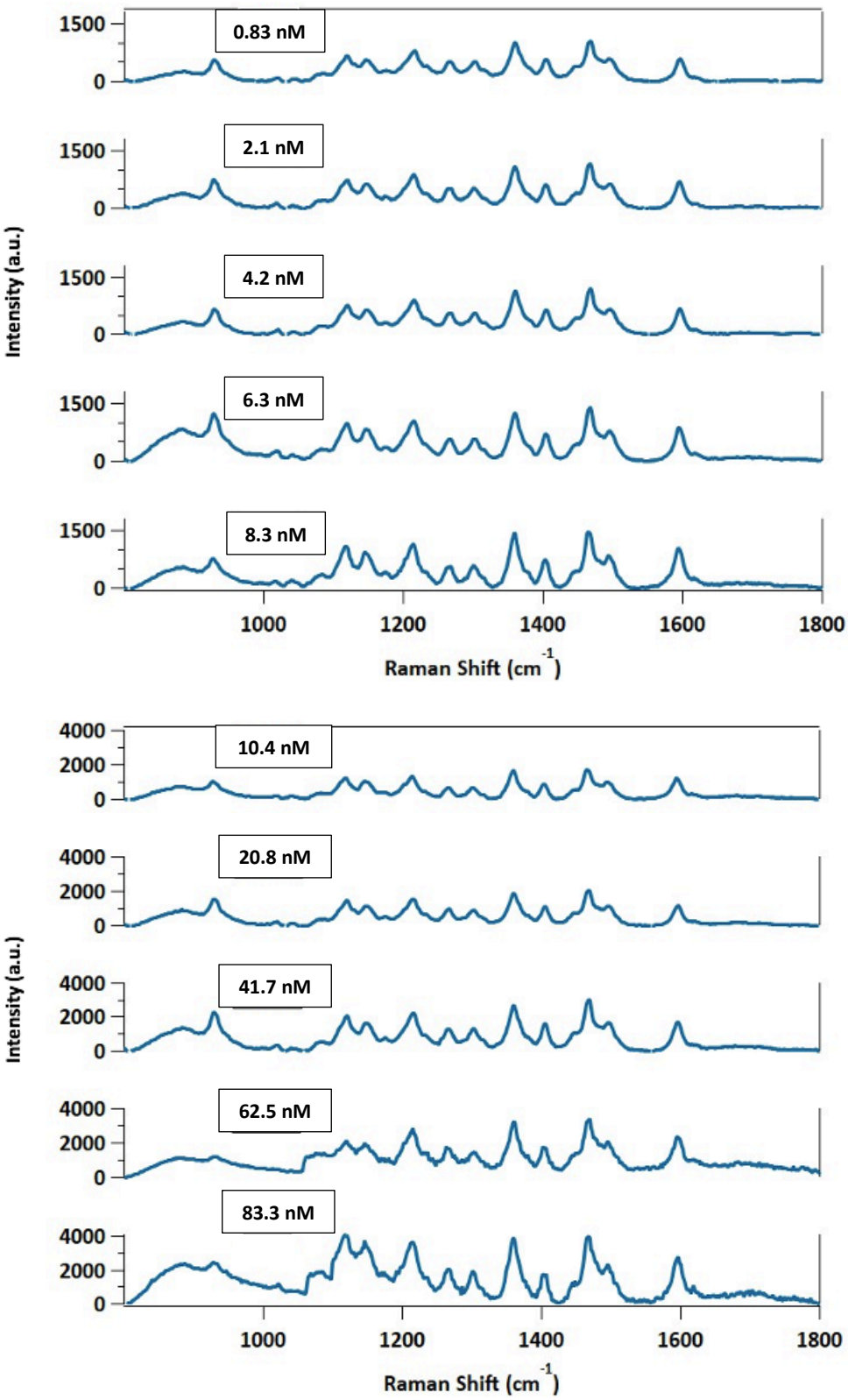

Figure C3. Stacked SERS spectra of Cy5 PEG RP **blood** hybridizations at concentrations within LDR.

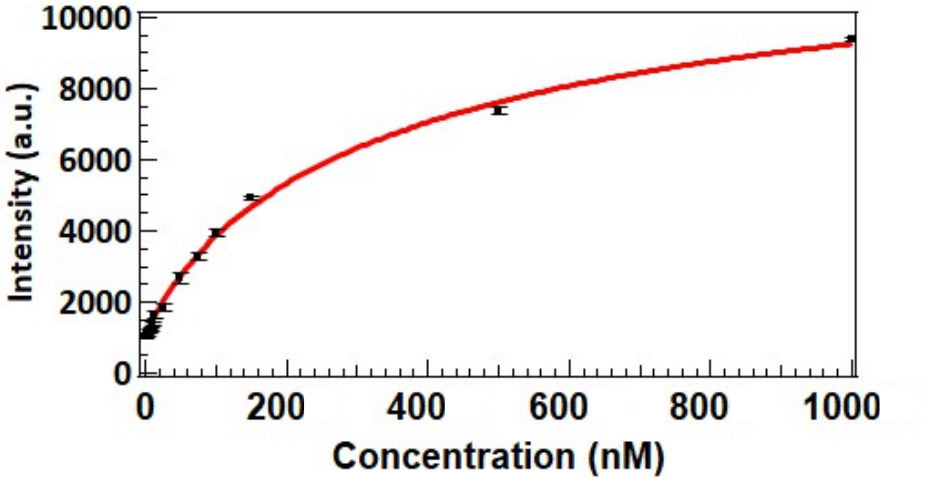

Figure C4. Hill-Langmuir fitting over entire range of concentrations tested in Cy5 RP **blood** hybridizations. LDR determined from tangent line at inflection point of Hill-Langmuir fit.